nature immunology

ARTICLES

https://doi.org/10.1038/s41590-017-0043-5

Tumor-derived exosomes antagonize innate antiviral immunity

Liang Gao[1,2], Lin Wang[2], Tong Dai[1,2], Ke Jin[1], Zhengkui Zhang[1], Shuai Wang[2], Feng Xie[1,2], Pengfei Fang[1], Bing Yang[5], Huizhe Huang[4], Hans van Dam[3], Fangfang Zhou[2*] and Long Zhang[1*]

Malignancies can compromise innate immunity, but the mechanisms of this are largely unknown. Here we found that, via tumor-derived exosomes (TEXs), cancers were able to transfer activated epidermal growth factor receptor (EGFR) to host macrophages and thereby suppress innate antiviral immunity. Screening of the human kinome identified the kinase MEKK2 in macrophages as an effector of TEX-delivered EGFR that negatively regulated the antiviral immune response. In the context of experimental tumor implantation, MEKK2-deficient mice were more resistant to viral infection than were wild-type mice. Injection of TEXs into mice reduced innate immunity, increased viral load and increased morbidity in an EGFR- and MEKK2-dependent manner. MEKK2 phosphorylated IRF3, a transcription factor crucial for the production of type I interferons; this triggered poly-ubiquitination of IRF3 and blocked its dimerization, translocation to the nucleus and transcriptional activity after viral infection. These findings identify a mechanism by which cancer cells can dampen host innate immunity and potentially cause patients with cancer to become immunocompromised.

After infection, germline-encoded pattern-recognition receptors recognize pathogen-associated molecular patterns of invading viruses and initiate a series of signaling pathways that lead to the production of type I interferons and proinflammatory cytokines[1,2]. Pattern-recognition receptors that recognize these viral nucleic acids include TLRs[3], RIG-I-like receptors[4–7] and certain DNA sensors such as cGAS and IFI16[8,9]. Following the recognition of viral nucleic acid, the pattern-recognition receptors recruit downstream adaptors, including TRIF, MAVS and STING[10–12]. Those adaptors subsequently activate the downstream kinases TBK1 and IKKε. TBK1 and IKKε then activate the transcription factors NF-κB and IRF3, which translocate to the nucleus and induce the expression of type I interferons, a family of cytokines that are essential for host protection[13–15].

Exosomes are small membraned vesicles (30–100 nm in diameter) synthesized in late endosomes and released into the extracellular milieu by various cell types[16,17]. Exosomes contain functional biomolecules (proteins, lipids, RNA and DNA) that can be transferred horizontally to recipient cells[18–21]. Tumor-derived exosomes (TEXs) are emerging as regulators of tumorigenesis. Exosomes secreted from melanomas reprogram bone marrow progenitor cells toward a pro-vasculogenic phenotype in the pre-metastatic niche[22]. TEXs are associated with the recruitment of neutrophils and eosinophils, the proliferation of natural killer cells and the activation of macrophages, which are involved in adaptation of the cancer microenvironment[23]. Specific proteins present in exosomes have been reported to determine organ-specific metastasis and the survival of patients with cancer[24,25]. In addition, TEXs deliver to immune cells suppressive or activating molecular signals, which directly or indirectly influence the development, maturation and antitumor activity of the cells[26–28]. However, whether TEXs influence innate antiviral immunity in the host is unknown.

We found here that TEXs were able to transfer activated epidermal growth factor receptor (EGFR) to host macrophages, which engaged a macrophage-intrinsic signaling pathway that reduced their production of type I interferons and antiviral immunity. These results demonstrate a mechanism by which tumor cells can cause immunocompromised host immunity.

Results

TEXs dampen innate antiviral immunity. Among patients with influenza, those without cancer showed a significantly higher concentration of serum interferon-β (IFN-β) than that of those with lung cancer who were not on chemotherapy (Fig. 1a); this suggested that IFN-β signaling might be impaired by lung cancer. To investigate whether tumor growth can affect innate antiviral immunity in the host, we cultured RAW264.7 mouse macrophages together with mouse Lewis lung cancer (LLC) cells or non-cancerous mouse lung fibroblasts (MLFs) (control cells), using polycarbonate membrane inserts to avoid direct contact between the two cell types. Secretion of IFN-β induced by the RNA virus Sendai virus (SeV) or the DNA virus herpes simplex virus type 1 (HSV-1) was significantly lower in RAW264.7 cells cultured with LLC cells than in 'homogeneously' cultured RAW264.7 cells (cultured alone) or RAW264.7 cells cultured with MLFs (Fig. 1b). Culture of THP-1 human monocytic cells with A549 human alveolar basal epithelial cells produced results similar to those obtained for the culture of RAW264.7 cells with LLC cells (Supplementary Fig. 1a,b). Knockdown of Rab27a, a protein required for the secretion of exosomes, significantly reduced the inhibitory effect of A549 cells or LLC cells on the antiviral response of the THP-1 cells or Raw264.7 cells, respectively, with which they were cultured (*$P < 0.05$ (two-tailed Student's t-test); Supplementary Fig. 1c). Pre-treatment of A549 cells or LLC cells with dimethyl amiloride, which inhibits the release of exosomes,

[1]Life Sciences Institute and Innovation Center for Cell Signaling Network, Hangzhou, Zhejiang, China. [2]Institutes of Biology and Medical Sciences, Soochow University, Suzhou, China. [3]Department of Molecular Cell Biology, Cancer Genomics Centre Netherlands, Leiden University Medical Center, Leiden, The Netherlands. [4]Faculty of Basic Medical Sciences, Chongqing Medical University, Chongqing, China. [5]Department of Pharmaceutical Chemistry and the Cardiovascular Research Institute, University of California San Francisco, San Francisco, CA, USA. Liang Gao, Lin Wang, Tong Dai, Ke Jin and Zhengkui Zhang contributed equally to this work. *e-mail: zhoufangfang@suda.edu.cn; l_zhang@zju.edu.cn

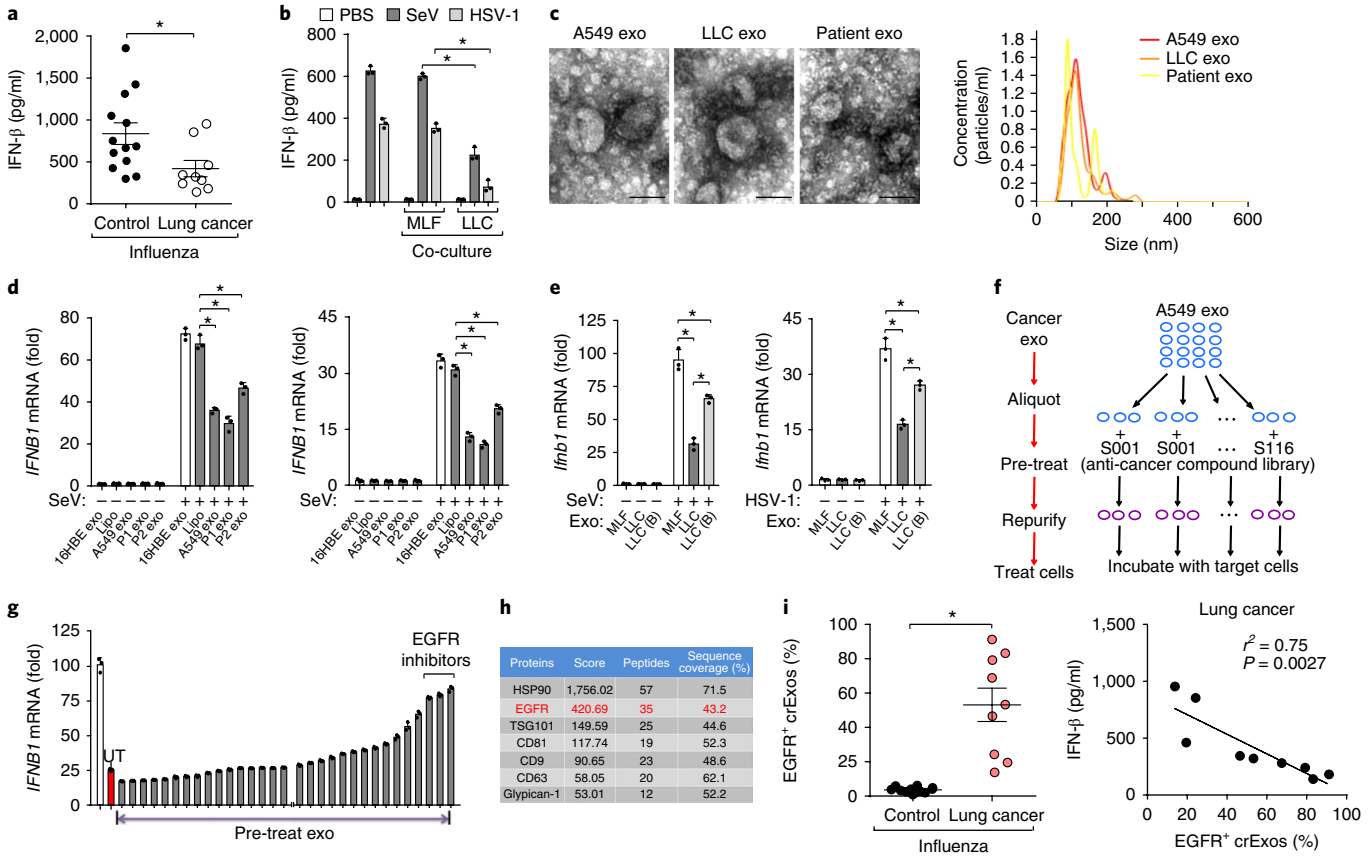

Proteins	Score	Peptides	Sequence coverage (%)
HSP90	1,756.02	57	71.5
EGFR	420.69	35	43.2
TSG101	149.59	25	44.6
CD81	117.74	19	52.3
CD9	90.65	23	48.6
CD63	58.05	20	62.1
Glypican-1	53.01	12	52.2

Fig. 1 | TEXs repress the innate antiviral response. a, ELISA of IFN-β in serum of patients with influenza but no cancer (Control (left); $n = 13$) or patients with lung cancer and influenza (right; $n = 9$). **b**, ELISA of IFN-β in supernatants of primary peritoneal macrophages cultured for 24 h with MLFs or LLC cells (below plot) or not (left three bars), followed by incubation for 8 h with PBS (control), SeV or HSV-1 (MOI (multiplicity of infection), 10) (key). **c**, Electron microscopy images of exosomes secreted by A549 cells (A549 exo), LLC cells (LLC exo) or patient-derived primary lung cancer cells (Patient exo) (left), and nanoparticle tracking of exosomes from those cells (key) (right). Scale bars (left), 100 nm. **d**,**e**, qPCR analysis of *IFNB1* mRNA in THP-1 cells pre-treated for 24 h with empty liposomes (Lipo) or with exosomes (40 μg) derived from 16HBE human bronchial epithelial cells (as a control; 16HBE exo), A549 cells (A549 exo) or primary lung cancer cells (P1 exo or P2 exo) (**d**) or of *Ifnb1* in primary peritoneal macrophages pre-treated with exosomes derived from MLFs (as a control) or derived from LLC cells and left untreated or boiled (B) (**e**), followed by no stimulation (−) or stimulation (+) for 8 h with SeV (left) or HSV-1 (right) (MOI, 10); results are presented relative to those of the control gene *GAPDH* (**d**) or *Gapdh* (**e**). **f**, Screening procedure for exosome components critical for the innate antiviral response. **g**, qPCR analysis of *IFNB1* mRNA in THP-1 cells incubated without (far left; open bar) or with (gray bars) aliquots of A549 exosomes (40 μg) left untreated (UT) (red) or pre-treated for 24 h with anti-cancer compounds, followed by stimulation for 8 h with SeV; results presented as in **d**. **h**, Mass-spectrometry analysis of exosomes secreted by A549 cells, showing results for the heat-shock protein HSP90, EGFR (red), TSG101, the tetraspanin integral membrane protein CD81, the integrin signaling modulator CD9 and the heparan sulfate proteoglycan glypican-1. **i**, Frequency of EGFR$^+$ crExos in samples as in **a** (left), and correlation between IFN-β in serum and frequency of EGFR$^+$ crExos (right). Each symbol (**a**,**i**) represents an individual subject; small horizontal lines indicate the mean (± s.d.) of technical triplicates. *$P < 0.05$ (two-tailed Student's *t*-test). Data are representative of at least two independent experiments (mean + s.d. of technical triplicates in **b**,**d**,**e**,**g**).

also counteracted the inhibitory effect of these cells on the antiviral response of the macrophages or monocytes with which they were cultured (Supplementary Fig. 1d). These results suggested that the cancer cells were able to inhibit the antiviral immunity of the macrophages by secreting exosomes. To investigate this further, we isolated exosomes from A549 cells and LLC cells, as well as from patient-derived primary lung cancer cells and MDA-MB-231 human breast cancer cells (Fig. 1c and data not shown). Pre-treatment of THP-1 cells with these (tumor-derived) exosomes significantly diminished the abundance of SeV- or HSV-1-induced *IFNB1* mRNA (Fig. 1d and Supplementary Fig. 1e). Heat denaturation reduced this inhibitory effect of TEXs (Fig. 1e), which indicated that protein components included in TEXs were important in this. To determine which protein(s) was (were) critical for the TEX-mediated innate immunosuppression, we treated A549 cell–derived exosomes with a library of 116 small-molecule anti-cancer compounds that target key oncogenic proteins (Fig. 1f). Of note, A549 cell–derived TEXs pre-treated with EGFR inhibitors lost their ability to repress the antiviral response of THP-1 cells (Fig. 1g). Mass spectrometry confirmed that EGFR was abundantly present in both exosomes derived from A549 cells and those from MDA-MB-231 cancer cells (Fig. 1h and Supplementary Fig. 1f), but not in exosomes derived from normal lung fibroblasts (MLFs). Immunoblot analysis showed that cancer exosomes showed enrichment for activated EGFR phosphorylated at Tyr1068 (p-EGFR) (Supplementary Fig. 1g). Immunogold transmission electron microscopy revealed that many of the p-EGFR molecules in the TEXs were anchored to the membrane (Supplementary Fig. 1h). Flow cytometry of these TEXs showed that more than 50% of the exosomes from A549 cells were positive for EGFR (Supplementary Fig. 1i). EGFR was hardly present at all in immune cells such as THP-1 cells, primary peritoneal macrophages and bone marrow–derived macrophages treated with

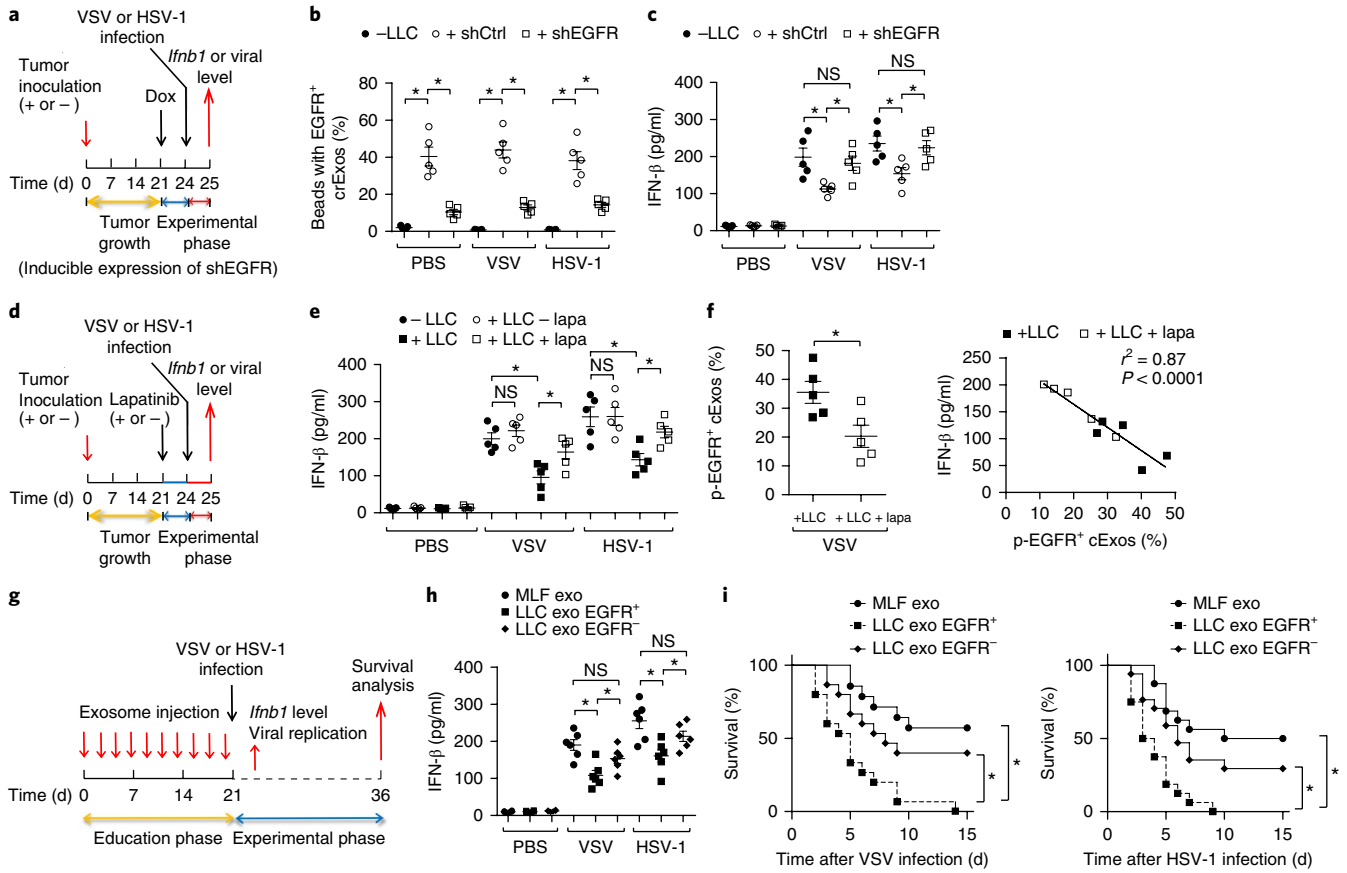

Fig. 2 | EGFR activity is required for tumor- and TEX-induced suppression of immunity. a, Experimental analysis in vivo: mice were not inoculated (−) or were given subcutaneous inoculation (+) of LLC cells (2×10^6 cells per mouse) expressing control shRNA or doxycycline-inducible shRNA targeting EGFR (shEGFR) (top left) and tumors were grown for 3 weeks, followed by the administration of doxycycline (DOX); 3 d later, mice were given intraperitoneal injection of PBS or VSV (5×10^8 PFU per mouse) or intranasal administration of HSV-1 (2×10^7 PFU per mouse), followed by further analysis 24 h later. **b**, Frequency of EGFR$^+$ crExos in PBS-treated (control) or virus-infected mice (horizontal axis) given inoculation of LLC cells expressing control shRNA (+ shCtrl) or doxycycline-inducible shEGFR (+ shEGFR) or not (– LLC) (key) as in **a**. **c**, ELISA of IFN-β in the serum of mice as in **a** ($n=5$ per group). **d**, Experimental procedure in vivo: mice were given inoculation (or not) of LLC cells (2×10^6 cells per mouse) (top left), followed by intraperitoneal injection of PBS or lapatinib (25 mg per kg body weight, twice per day); 3 d later, mice were infected with PBS, VSV or HSV-1 as in **a**. **e**, ELISA of IFN-β in the serum of mice ($n=5$ per group) given inoculation of LLC cells (+ LLC) or not (– LLC), followed by injection of PBS or lapatinib (+ lapa) (key) and then infection (horizontal axis) as in **d**. **f**, Frequency of p-EGFR$^+$ crExos in tumor-inoculated (+ LLC) mice treated with lapatinib (+ lapa) or not (horizontal axis) and infected with VSV (below plot) as in **d** (left), and correlation between IFN-β in serum and p-EGFR$^+$ crExos in mice as at left (right). **g**, Exosome administration and experimental analysis in vivo: mice were given injection (into the tail vein) of exosomes (50 μg per mouse every other day) derived from MLFs or LLC cells (EGFR$^+$ or EGFR$^-$), followed by infection with PBS, VSV or HSV-1 as in **a**. **h**, ELISA of IFN-β in the serum of mice ($n=6$ per group) given injection of exosomes from MLFs, EGFR$^+$ LLC cells or EGFR$^-$ LLC cells (key), then infected as in **g** (horizontal axis). **i**, Survival of mice ($n=14$ per group) as in **g** (key) at various times (horizontal axis) after infection with VSV (left) or HSV-1 (right) as in **g**. Each symbol (**b**,**c**,**e**,**f**,**h**) represents an individual mouse; small horizontal lines indicate the mean (± s.d.) of technical replicates. NS, not significant ($P>0.05$); *$P<0.05$ (two-tailed Student's *t*-test (**b**,**c**,**e**,**f**,**h**) or two-way analysis of variance (**i**)). Data are representative of at least two independent experiments.

exosomes derived from non-cancerous cells (control exosomes), but after treatment with exosomes derived from cancer cells, activated EGFR accumulated in these immune cells (Supplementary Fig. 1j). By using an antibody that recognizes only human EGFR, we observed a sharp increase in the pool of mouse RAW264.7 cells positive for human EGFR on their cell surface after they were treated with exosomes from A549 cells (Supplementary Fig. 1k). Flow cytometry showed that the frequency of EGFR$^+$ circulating exosomes (crExos) was much higher in patients with lung cancer than in subjects without cancer (control subjects), in whom these were barely detectable (Fig. 1i). Moreover, in patients with lung cancer and influenza, IFN-β production was significantly inversely correlated with the abundance of EGFR$^+$ crExos. These results indicated that tumor cells might impair host innate antiviral immunity by secreting EGFR$^+$ exosomes.

EGFR is required for TEX-mediated innate antiviral immunosuppression. To confirm that EGFR released from TEXs was responsible for the suppression of antiviral responses in vivo, we used a doxycycline-regulated promoter to silence EGFR expression (via short hairpin RNA (shRNA)) in LLC cells; we inoculated mice with xenografts of those LLC cells and treated them with doxycycline 3 weeks after inoculation (Fig. 2a). Serum from non-inoculated mice revealed almost no positivity for EGFR in crExos (Fig. 2b), whereas the mice given LLC cell xenografts displayed EGFR$^+$ crExos ranging from 30% to 58% (average, 40%; Fig. 2b). Doxycycline-mediated transient loss of EGFR did not significantly alter tumor volume but sharply reduced the abundance of EGFR$^+$ crExos (Fig. 2b). After infection with the RNA virus vesicular stomatitis virus (VSV) or HSV-1, the concentration of IFN-β in the serum of mice given LLC cell xenografts was much lower than that

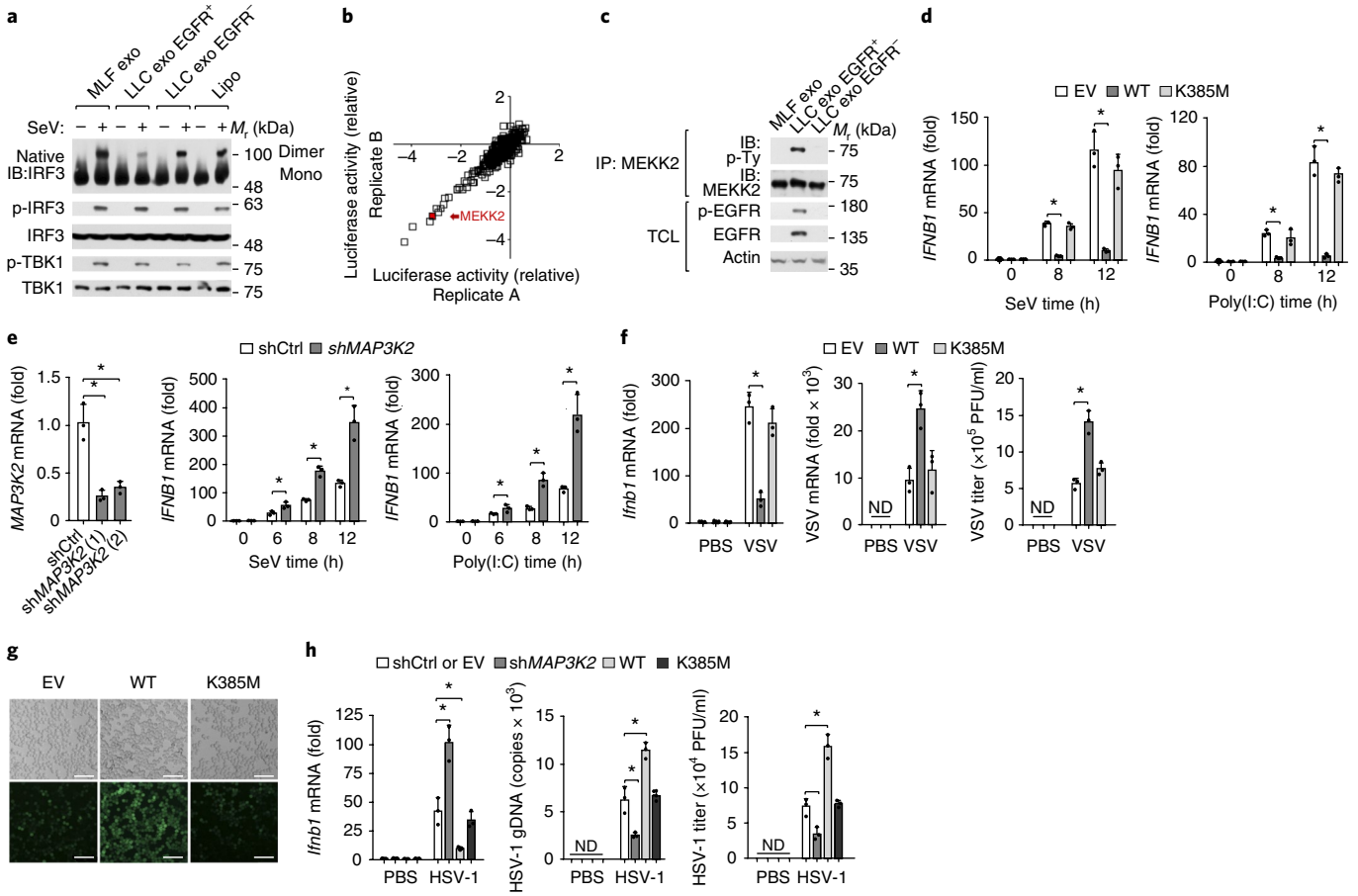

Fig. 3 | A human kinome screen identifies MEKK2 as a repressor of IFN-β signaling. a, Immunoblot analysis of monomeric (Mono) and dimeric (Dimer) IRF3 (top blot; native PAGE) and total lysates (bottom blot; denaturing gel) of primary peritoneal macrophages pre-treated for 24 h with empty liposomes or with exosomes (40 μg) derived from MLFs or EGFR$^+$ or EGFR$^-$ LLC cells (above blots), followed by infection for 8 h with SeV (+) or not (−) (above lanes). Right margin, relative molecular mass (M_r) in kilodaltons (kDa). **b**, IFN-β–luciferase (IFN-β-luc) reporter activity in a human kinome screen of SeV-infected HEK293T cells, assessing cDNA encoding 442 kinases (one per symbol; red, MEKK2) in two replicates (one per axis); results presented relative to firefly luciferase activity. $P < 0.01$ (two-tailed Student's *t*-test). **c**, Immunoblot analysis (IB) of phosphorylated tyrosine (p-Ty) or MEKK2 among proteins immunoprecipitated (IP) from primary peritoneal macrophages pre-treated with exosomes as in **a** (above lanes) (top), and of phosphorylated (p-) and total EGFR and actin (loading control) in total lysates of those cells (TCL) (bottom). **d**,**e**, qPCR analysis of *IFNB1* mRNA in HEK293T cells transfected with empty vector (EV) or expression vector encoding wild-type MEKK2 or MEKK2 K385M (key) (**d**) or with control shRNA (shCtrl) or shRNA targeting the gene encoding MEKK2 (sh*MAP3K2*) (key) (**e**, middle and right) and stimulated for various times with SeV or poly (I:C) (horizontal axis), and qPCR analysis of *MAP3K2* mRNA in HEK293T cells transfected with control shRNA or either of two independent *MAP3K2*-specific shRNAs (sh*MAP3K2* (1) or sh*MAP3K2* (2)) (**e**, left); results are presented relative to those of *GAPDH*. **f**, qPCR analysis of *Ifnb1* mRNA (left) or VSV-specific mRNA (middle) and plaque assay of the VSV titer (right) in RAW264.7 cells transfected as in **d** (key) and stimulated for 8 h with VSV (MOI, 0.1) or not (PBS) (horizontal axis); qPCR results presented relative to those of *Gapdh*, and plaque assay results presented as plaque-forming units (PFU). **g**, Brightfield microscopy (top) and fluorescence microscopy (bottom) of VSV-GFP in HEK293T cells transfected with constructs as in **d** (above images), followed by infection for 18 h with VSV-GFP (MOI, 0.1). Scale bars, 100 μm. **h**, qPCR analysis of *Ifnb1* mRNA (left) or HSV-1-specific genomic DNA (gDNA) (middle) and plaque assay of the HSV-1 titer (right) in RAW264.7 cells transfected as in **d**,**e** (key) and stimulated for 8 h with HSV-1 (MOI, 10) or not (PBS) (horizontal axis); results presented relative to those of *Gapdh*. Each symbol (**d**,**e**,**f**,**h**) represents an individual technical replicate. *$P < 0.05$ (two-tailed Student's *t*-test). Data are representative of at least two independent experiments (mean + s.d. of technical triplicates in **d**,**e**,**f**,**h**).

in the serum of non-inoculated (control) mice, and loss of EGFR in the LLC tumor was able to restore the concentration of IFN-β (Fig. 2c). In line with those findings, both VSV titers in the lungs and HSV-1 titers in the brain were higher in mice given LLC cell xenografts than non-inoculated (control) mice, and loss of EGFR in tumor showed significantly suppressed titers of VSV and HSV-1 in mice given LLC cell xenografts (*$P < 0.05$ (two-tailed Student's *t*-test); Supplementary Fig. 2a). These results suggested that EGFR released from TEXs-suppressed innate antiviral immunity. We next used the EGFR inhibitor lapatinib to investigate whether EGFR activity was essential for this (Fig. 2d). Treatment with lapatinib significantly restored the concentration of IFN-β reduced by tumors and decreased the tumor-induced titers of VSV and HSV-1 in mice given LLC cell xenografts (Fig. 2e and Supplementary Fig. 2b). Treatment with lapatinib also significantly reduced the abundance of p-EGFR$^+$ crExos in mice given LLC cell xenografts, in which the abundance of p-EGFR$^+$ crExos was significantly inversely correlated with IFN-β production in both VSV-treated mice and HSV-1-treated mice (Fig. 2f and Supplementary Fig. 2c).

We next investigated whether the administration of EGFR$^+$ TEXs would be sufficient to cause innate antiviral immunosuppression both in vitro and in vivo. We deleted the gene encoding

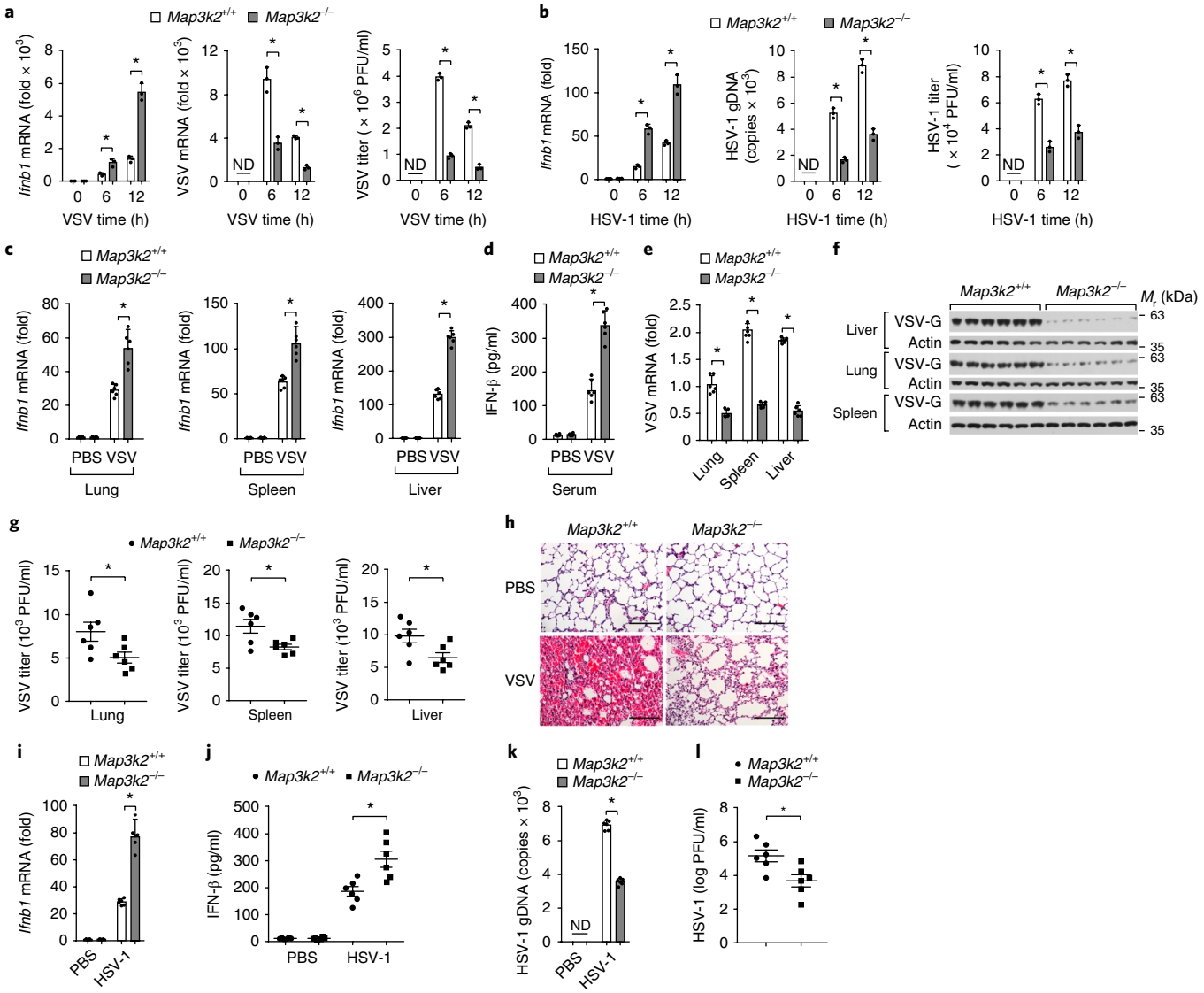

Fig. 4 | MEKK2 deficiency potentiates an innate antiviral response. a,**b**, qPCR analysis of *Ifnb1* mRNA (left) or VSV-specific mRNA or HSV specific genomic DNA (middle), and titer of VSV or HSV-1 (right), in *Map3k2*$^{+/+}$ and *Map3k2*$^{-/-}$ peritoneal macrophages (key) infected for various times (horizontal axis) with VSV (MOI, 0.1) (**a**) or HSV-1 (**b**) (MOI, 10); qPCR results are presented relative to those of *Gapdh*. **c**, qPCR analysis of *Ifnb1* mRNA in the lungs, spleen and liver (below plot) of *Map3k2*$^{+/+}$ and *Map3k2*$^{-/-}$ mice (key; $n = 6$ per group) given intraperitoneal injections of PBS or VSV (5×10^8 PFU per mouse) for 24 h; results presented as in **a**,**b**. **d**, ELISA of IFN-β in serum of mice as in **c**. **e**–**g**, qPCR analysis of VSV-specific mRNA (**e**), immunoblot analysis of VSV-G (**f**) and plaque assay of VSV (**g**) in the lungs, liver and spleen of the mice as in **c**. **h**, Microscopy of hematoxylin-and-eosin–stained lung sections from mice as in **c**. Scale bars, 100 μm. **i**, qPCR analysis of *Ifnb1* mRNA in the brain of mice ($n = 6$ per group) 24 h after intranasal administration of PBS or HSV-1 (2×10^7 PFU per mouse); results presented as in **a**,**b**. **j**, ELISA of IFN-β in the serum of the mice in **i**. **k**,**l**, qPCR analysis of HSV-1 genomic DNA (**k**) and plaque assay of HSV-1 (**l**) in the brain of the mice as in **i**; qPCR results presented as in **a**,**b**. Each symbol (**a**–**e**,**g**,**i**–**l**) represents an individual replicate (**a**,**b**) or mouse (**c**–**e**,**g**,**i**–**l**); small horizontal lines (**g**,**j**,**l**) indicate the mean (± s.d.). *$P < 0.05$ (two-tailed Student's *t*-test). Data are representative of at least two independent experiments (mean + s.d. in **a**–**e**,**i**,**k**).

EGFR in LLC cells by CRISPR-Cas9 technology and compared exosomes purified from the parental cells and those in which this gene was deleted. Immunoblot analysis confirmed that EGFR was absent in TEXs from the cells in which the gene encoding EGFR was deleted (Supplementary Fig. 3a). Pre-treatment of macrophages with EGFR$^+$ exosomes substantially inhibited the *Ifnb1* expression and IFN-β secretion stimulated by SeV or the synthetic RNA duplex poly (I:C) in the recipient macrophages, whereas pre-treatment with EGFR$^-$ exosomes had a much weaker effect (Supplementary Fig. 3b). Similarly, EGFR$^+$ exosomes considerably reduced the expression of *Ifnb1* in primary macrophages after infection with VSV, whereas EGFR$^-$ exosomes were much less effective in this (Supplementary Fig. 3c). Consistent with those results, we found higher levels of VSV-specific mRNA and VSV titers in macrophages treated with EGFR$^+$ exosomes than in cells treated with EGFR$^-$ exosomes (Supplementary Fig. 3c). Fluorescence microscopy of green fluorescent protein (GFP)-expressing VSV (VSV-GFP) showed that viral replication in recipient HEK293T human embryonic kidney cells was substantially increased by LLC cell–derived EGFR$^+$ exosomes, whereas LLC cell–derived EGFR$^-$ exosomes barely produced this effect at all (Supplementary Fig. 3d). In addition, EGFR$^+$ exosomes derived from LLC cells inhibited the HSV-1-induced *Ifnb1*

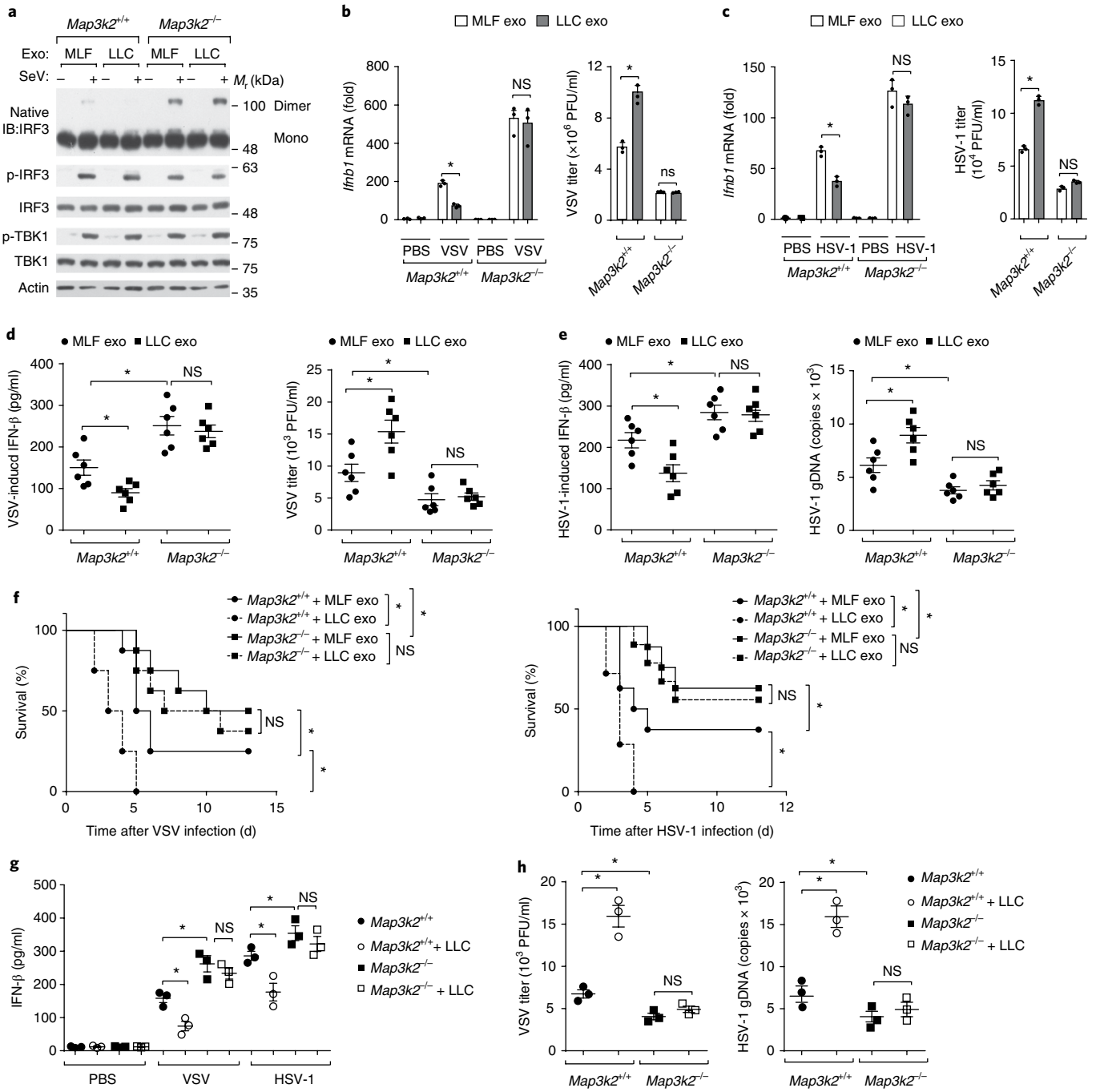

Fig. 5 | MEKK2 is required for TEX-induced innate antiviral immunosuppression. a, Immunoblot analysis of monomeric and dimeric IRF3 (native gel; top) and of phosphorylated and total IRF3 and TBK1 (below) in *Map3k2*$^{+/+}$ and *Map3k2*$^{-/-}$ peritoneal macrophages pre-treated for 24 h with exosomes (40 μg) derived from MLFs or LLC cells (above blots), followed by infection for 8 h with SeV (+) or not (–) (above lanes). **b**,**c**, qPCR analysis of *Ifnb1* mRNA (left) and plaque assay (right) of the titer of VSV (**b**) or HSV-1 (**c**) in *Map3k2*$^{+/+}$ and *Map3k2*$^{-/-}$ peritoneal macrophages pre-treated with exosomes as in **a** (key), followed by infection for 8 h with Sev (**b**) or HSV-1 (MOI, 10) (**c**) or not (PBS); qPCR results are presented relative to those of *Gapdh*. **d**,**e**, ELISA of IFN-β in the serum (left) and plaque assay of the titer of VSV (**d**) or HSV-1 (**e**) (right) in the lungs of *Map3k2*$^{+/+}$ and *Map3k2*$^{-/-}$ mice (horizontal axis; $n = 6$ per group) pre-treated with exosomes (key) and infected with virus as in Fig. 2d. **f**, Survival of *Map3k2*$^{+/+}$ and *Map3k2*$^{-/-}$ mice (key; $n = 8$ per group) pre-treated with exosomes (key), followed by infection with VSV (left) or HSV-1 (right) as in Fig. 2d. **g**, ELISA of IFN-β in the serum of *Map3k2*$^{+/+}$ and *Map3k2*$^{-/-}$ mice (key; $n = 3$ per group) inoculated with LLC cells (+ LLC) or not (key) and infected with virus as in Fig. 2a. **h**, Plaque assay of the titer of VSV in the lungs (left) and HSV-1 in the brain (right) of mice as in **g**. Each symbol (**b**–**e**,**g**,**h**) represents an individual replicate (**b**,**c**) or mouse (**d**,**e**,**g**,**h**); small horizontal lines (**d**,**e**,**g**,**h**) indicate the mean (± s.d.). *$P < 0.05$ (two-tailed Student's *t*-test (**b**,**c**–**e**,**g**,**h**) or two-way analysis of variance (**f**)). Data are representative of at least two independent experiments (mean + s.d. of technical triplicates in **b**,**c**).

mRNA and potentiated HSV-1 replication in primary peritoneal macrophages, whereas EGFR$^-$ exosomes did not have this effect (Supplementary Fig. 3e).

To determine whether TEXs regulate the antiviral innate immunity of the host in vivo, we injected LLC cell–derived TEXs into the tail vein of mice for 3 weeks and then challenged the mice with VSV

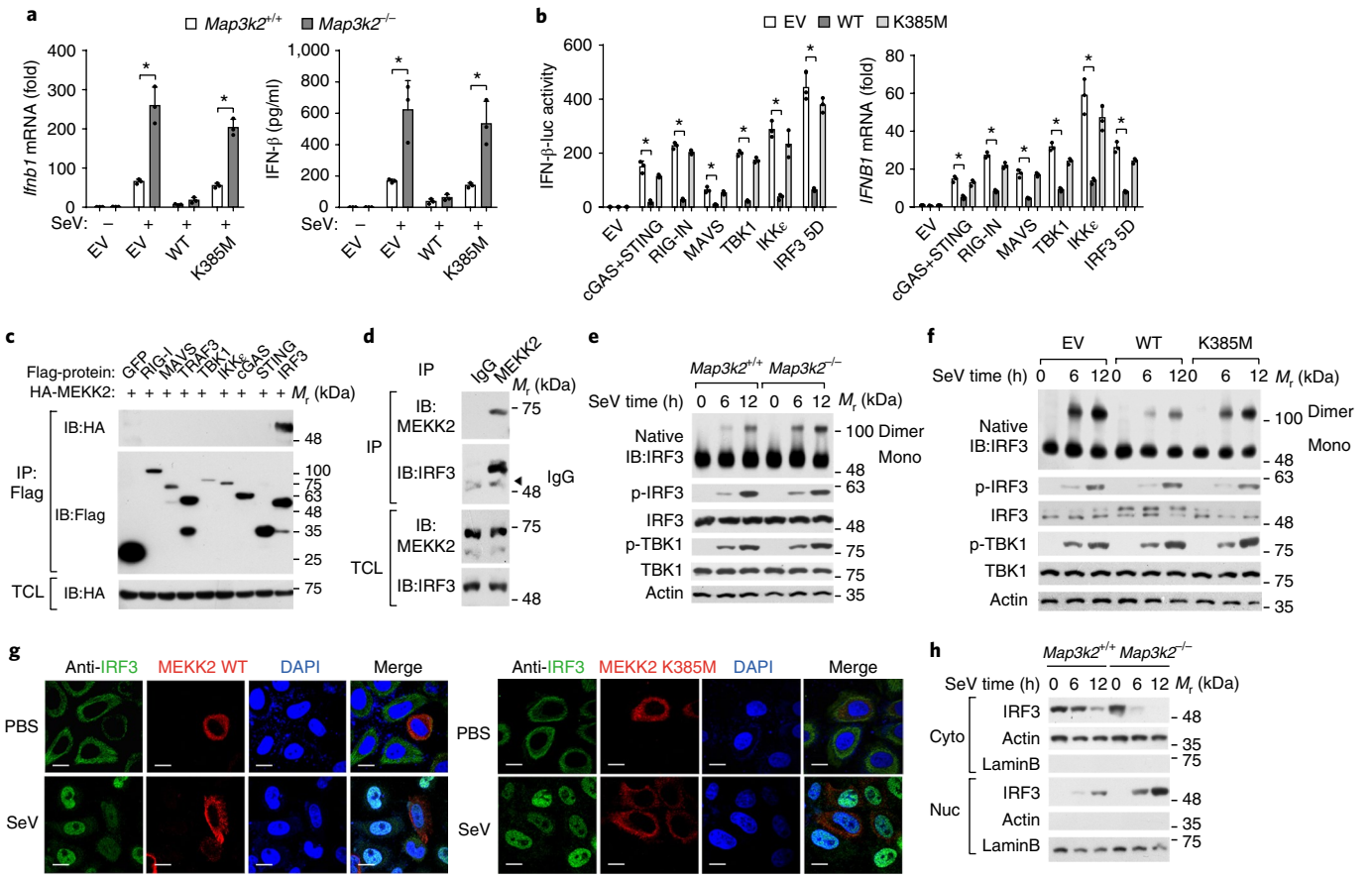

Fig. 6 | MEKK2 interferes with IRF3 activation. a, qPCR analysis of *Ifnb1* mRNA (left) and ELISA of IFN-β (right) in *Map3k2*$^{+/+}$ and *Map3k2*$^{-/-}$ peritoneal macrophages (key) transfected with empty vector (EV) or vector encoding wild-type MEKK2 (WT) or MEKK2 K385M (key), followed by mock infection (–) or infection with SeV (+) for 8 h; qPCR results are presented relative to those of *Gapdh*. **b**, IFN-β–luciferase activity (left) and *IFNB1* mRNA (right) in HEK293T cells transfected with constructs as in **a** (key) together with empty vector or expression plasmid(s) encoding cGAS plus STING, the RIG-I amino-terminal '2CARD' domain (RIG-IN), MAVS, TBK1, IKKε or IRF3-5D (horizontal axis); mRNA results are presented relative to those of *GAPDH*. **c**, Immunoblot analysis of proteins immunoprecipitated (IP) from HEK293T cells transfected with expression plasmids encoding HA-tagged MEKK2 and Flag-tagged GFP, RIG-I, MAVS, TRAF3, TBK1, IKKε, cGAS, STING or IRF3 (above lanes) (top two blots), and of total lysates of those cells (bottom). **d**, Immunoblot analysis of proteins immunoprecipitated from primary peritoneal macrophages with the control antibody IgG1 or with antibody to MEKK2 (above lanes) (top half), and of total lysates of those cells (below). **e**,**f**, Immunoblot analysis of monomeric and dimeric IRF3 (native gel; top) and of phosphorylated and total IRF3 and TBK1 (below) in *Map3k2*$^{+/+}$ and *Map3k2*$^{-/-}$ peritoneal macrophages (**e**) or A549 cells transfected with constructs as in **a** (**f**), all infected for 0, 6 or 12 h (above lanes) with SeV. **g**, Immunofluorescence and nuclear staining of HeLa cells transfected to express HA-tagged wild-type MEKK2 (left) or MEKK2 K385M (right) (above images) and treated for 8 h with PBS or SeV (left margin), then stained with antibody to IRF3 (Anti-IRF3) and the DNA-binding dye DAPI (above images). Scale bars, 10 μm. **h**, Immunoblot analysis of IRF3, as well as actin (cytoplasmic control) and laminin B (LaminB) (nuclear control), in nuclear (Nuc) and cytoplasmic (Cyto) fractions (left margin) of *Map3k2*$^{+/+}$ and *Map3k2*$^{-/-}$ MEFs (above blots) infected for 0, 6 or 12 h (above lanes) with SeV. Each symbol (**a**,**b**) represents an individual replicate. *$P < 0.05$ (two-tailed Student's *t*-test). Data are representative of at least two independent experiments (mean + s.d. of technical triplicates in **a**,**b**).

or HSV-1 (Fig. 2g). The VSV- or HSV-1-induced concentration of IFN-β was lower in the serum of mice exposed to EGFR$^+$ exosomes than in that of mice-exposed to EGFR$^-$ exosomes (Fig. 2h). Accordingly, the amount of VSV-specific mRNA and VSV titers in the lungs, spleen and liver, as well as the abundance of HSV-1 specific genomic DNA and HSV-1 replication in the brain, were higher in the mice 'educated' with EGFR$^+$ exosomes than in mice treated with EGFR$^-$ exosomes (Supplementary Fig. 3f–h). Furthermore, mice pre-treated with EGFR$^+$ exosomes from LLC cells were more sensitive to infection with VSV and HSV-1 than were mice pre-treated with exosomes from MLFs or EGFR$^-$ exosomes (Fig. 2i). These results indicated an important role for EGFR delivered by TEXs in shutting off host innate immunity to both RNA viruses and DNA viruses.

Exosomal EGFR activates host MEKK2 to diminish IFN-β production. Next we sought to determine the mechanism by which the EGFR$^+$ exosomes impaired innate antiviral responses. Pre-treatment of peritoneal macrophages with LLC cell–derived EGFR$^+$ exosomes inhibited the dimerization of IRF3 but had no effect on the amount of IRF3 phosphorylated at Ser396 (p-IRF3) or TBK1 phosphorylated at Ser172 (p-TBK1) in recipient peritoneal macrophages, in contrast to results obtained with control liposomes or MLF-derived exosomes (Fig. 3a). This indicated that EGFR$^+$ exosomes might impair IFN-β signaling at the level of IRF3 dimerization. Since the main downstream effectors of activated EGFR are kinase cascades, we screened a cDNA library encoding the human kinome for effects on the activity of the promoter of the gene encoding IFN-β and on the dimerization of IRF3. Among the

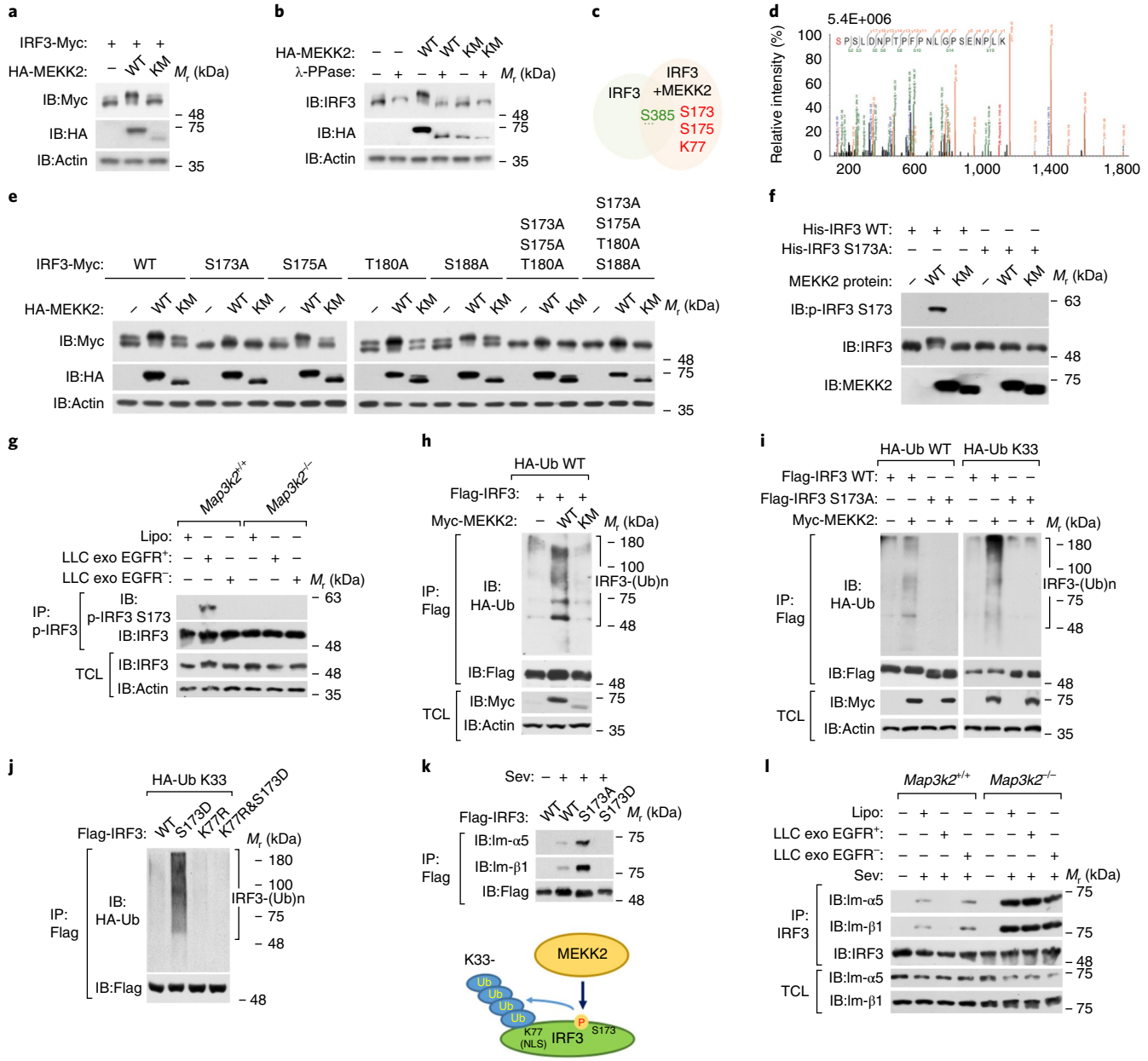

Fig. 7 | MEKK2 inhibits the function of IRF3 via phosphorylation of IRF3 at Ser173. a,**b**, Immunoblot analysis of lysates of HEK293T cells expressing Myc-tagged IRF3 (**a**) or not (**b**), left untransfected (–) or transfected with expression plasmid encoding HA-tagged wild-type MEKK2 (WT) or MEKK2 K385M (KM) (**a**,**b**), and left untreated (**a**) or treated with λ-phosphatase (λ-PPase) (**b**). **c**, Amino acids of IRF3 phosphorylated by MEKK2 (orange shaded area), as identified by mass spectrometry, and overlap with previously known phosphorylation sites. **d**, Mass spectrometry of the peptide containing MEKK2-phosphorylated IRF3 Ser173. **e**, Immunoblot analysis of lysates of HEK293T cells transfected with expression vector(s) encoding Myc-tagged wild-type IRF3 (WT) or IRF3 point mutants (above blots), along with vector encoding HA-tagged MEKK2 as in **a**,**b** (above lanes). **f**, Immunoblot analysis of purified His-tagged wild-type IRF3 or IRF3 S173A (grid above blots) incubated with purified wild-type MEKK2 or MEKK2 K385M or not (–) (above lanes), in the presence of unlabeled ATP. **g**, Immunoblot analysis of proteins immunoprecipitated from *Map3k2*$^{+/+}$ and *Map3k2*$^{-/-}$ peritoneal macrophages (above blots) incubated for 24 h with liposomes or with exosomes derived from EGFR^{+} or EGFR^{-} LLC cells (40 μg) (grid above blots) (top half), and of total lysates of those cells (bottom half). **h**,**i**, Immunoblot analysis of proteins immunoprecipitated from HEK293T cells expressing HA-tagged wild-type ubiquitin (HA-Ub WT) (**h**) or HA-tagged K33-linked ubiquitin (HA-Ub K33) (**i**) and transfected with plasmid(s) encoding Flag-tagged wild-type IRF3 (**h**,**i**) or IRF3 S173A (**i**)) and Myc-tagged wild-type MEKK2 (**h**,**i**) or MEKK2 K385M (**h**) (above lanes) (top half), and of total lysates of those cells (bottom half). **j**, Immunoblot analysis of proteins immunoprecipitated from HEK293T cells expressing HA-tagged K33-linked ubiquitin, transfected to express Flag-tagged wild-type IRF3 or IRF3 point mutants (above lanes). **k**, Immunoblot analysis (top) of proteins immunoprecipitated (with anti-Flag) from HeLa cells transfected to express Flag-tagged wild-type IRF3 or IRF3 point mutants (above lanes) and infected with SeV (+) or not (–); below, proposed effects of MEKK2 on IRF3. **l**, Immunoblot analysis of proteins immunoprecipitated from *Map3k2*$^{+/+}$ and *Map3k2*$^{-/-}$ macrophages incubated with liposomes or exosomes as in **g** (grid above blot), followed by infection for 8 h with SeV (+) or not (–) (above lanes) (top three blots), and of total lysates of those cells (below). Data are representative of three experiments (**a**,**b**), one experiment (**d**) or two experiments (**e**–**l**).

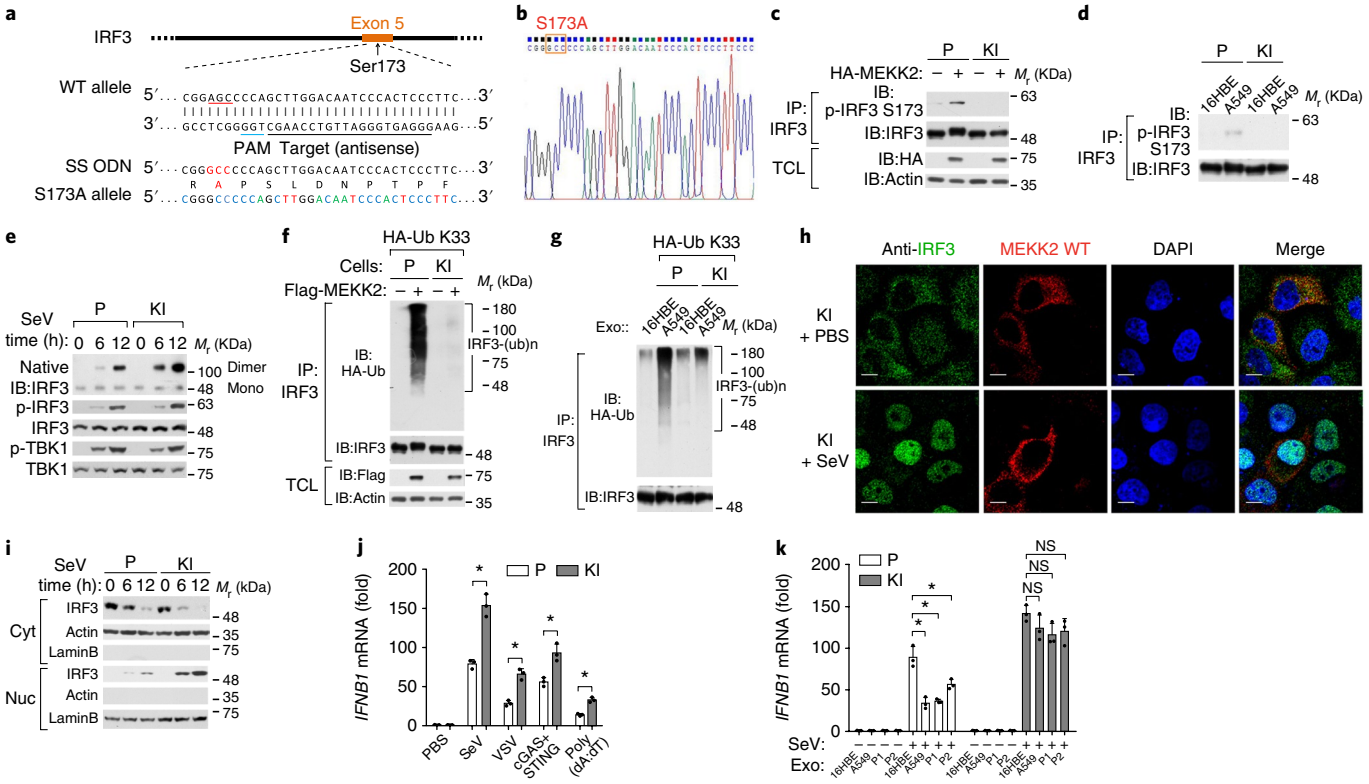

Fig. 8 | Ser173 of IRF3 is critical for IFN-β signaling and innate antiviral immunity. a, Design of guide RNA for CRISPR-Cas9 mutation of both copies of *IRF3* replacing Ser173 (AGC; underlined in wild-type allele) with alanine (GCC; red in oligodeoxynucleotide (SS ODN)); blue and green indicate mutated nucleotides. **b**, Sequencing verification of the IRF3 S173A replacement. **c**,**d**, Immunoblot analysis of proteins immunoprecipitated from parental (P) or S173A-KI (KI) HEK293T cells (above blots) transfected with expression vector encoding HA-tagged MEKK2 (+) or not (–)(above lanes) (**c**) or treated with exosomes derived from 16HBE cells (as a control) or A549 cells (above lanes) (**d**) (**c**, top half, and **d**), and of total lysates of those cells (**c**, bottom). **e**, Immunoblot analysis of monomers and dimers of IRF3 (native gel; top) in parental or S173A-KI HEK293T cells (above blots) infected for 0, 6 or 12 h (above lanes) with SeV. **f**,**g**, Immunoblot analysis of proteins immunoprecipitated (with anti-IRF3) from parental or S173A-KI HEK293T cells (above blots) expressing HA-tagged K33-linked ubiquitin, transfected with vector encoding Flag-tagged MEKK2 (+) or not (–) (above lanes) (**f**) or treated with exosomes derived from 16HBE or A549 cells (above lanes) (**g**). **h**, Immunofluorescence and DAPI staining, as well as staining with antibody to IRF3 (above images), of S173A-KI HeLa cells treated for 6 h with PBS or SeV (left margin). Scale bars, 20 μm. **i**, Immunoblot analysis of nuclear and cytoplasmic fractions (left margin) of parental and S173A-KI HEK293T cells (above blots) infected for 0, 6 or 12 h (above lanes) with SeV. **j**,**k**, qPCR analysis of *IFNB1* mRNA in parental and S173A-KI HeLa cells (key) given no pretreatment (**j**) or pre-treated with exosomes from 16HBE cells, A549 cells or primary lung cancer cells (P1 or P2) (below plot) (**k**), followed by infection with PBS or SeV or VSV (MOI, 0.1) or transfection with expression plasmids encoding cGAS and STING or with poly(dA:dT); qPCR results are presented relative to those of *GAPDH*. Each symbol (**j**,**k**) represents an individual replicate. $^*P < 0.05$ (two-tailed Student's *t*-test). Data are representative of at least two independent experiments (mean + s.d. of technical triplicates in **h**,**i**).

445 kinases tested, 12 kinases showed a strong inhibitory effect on SeV-induced activity of the promoter of the gene encoding IFN-β (Supplementary Dataset 1), and among those, only MEKK2 and the serine-threonine kinases STK4 and STK24 were able to antagonize the SeV-induced dimerization of IRF3 (Fig. 3b and Supplementary Fig. 4a). EGFR$^+$ TEXs induced tyrosine phosphorylation of endogenous MEKK2, but not of STK4 or STK24, in primary peritoneal macrophages, but EGFR$^-$ TEXs did not (Fig. 3c). MEKK2 is a mitogen-activated protein kinase kinase kinase involved in activation of the kinase ERK5 ('extracellular signal–regulated kinase 5') and kinase JNK pathways[29]. MEKK2 can be activated through tyrosine phosphorylation in response to EGF[30,31], while transient expression of MEKK2 leads to its auto-activation[32]. To determine whether EGFR$^+$ TEXs could stimulate MEKK2 in vivo, we injected LLC cell–derived TEXs into the tail vein of mice for 3 weeks and then challenged the mice with VSV (Supplementary Fig. 4b). Analysis of macrophages from these mice exposed to TEXs revealed tyrosine phosphorylation of the host MEKK2 by EGFR delivered via TEXs (Supplementary Fig. 4b). EGFR$^+$ TEXs substantially blocked VSV-induced IRF3 dimerization in vivo, but EGFR$^-$ TEXs did not (Supplementary Fig. 4b).

We next investigated whether MEKK2 regulates the antiviral response. Depleting cells of the gene encoding MEKK2, through the use of shRNA targeting that gene, significantly upregulated the SeV- or poly (I:C)-induced activity of a reporter for the promoter of the gene encoding IFN-β and that of the PRD I–III reporter (containing only the IRF3-binding site of the promoter of the gene encoding IFN-β), relative to such activity in cells transfected with non-targeting (control) shRNA (Supplementary Fig. 4c). Overexpression of MEKK2 considerably inhibited the SeV- or poly (I:C)-induced activity of those reporters, whereas expression of a MEKK2 mutant (K385M) lacking kinase activity ('kinase-dead') did not have this effect (Supplementary Fig. 4d). In line with those findings, in both HEK293T cells and HeLa human cervical cancer cells, the SeV- or poly (I:C)-induced abundance of *Ifnb1* mRNA was downregulated by expression of wild-type MEKK2 and was upregulated by depleting cells of MEKK2, but it was not affected by the kinase-dead mutant MEKK2

K385M (Fig. 3d,e and Supplementary Fig. 4e,f). After challenge with VSV, *Ifnb1* expression was inhibited and the abundance of VSV-specific mRNA and VSV titers were increased by wild-type MEKK2 but not by MEKK2 K385M (Fig. 3f). In contrast, depleting cells of MEKK2 potentiated the VSV-induced *Ifnb1* expression and suppressed the abundance of VSV-specific mRNA and VSV titers (Supplementary Fig. 4g). The replication of VSV-GFP was accordingly increased by ectopic expression of wild-type MEKK2 and was reduced after depletion of MEKK2, whereas MEKK2 K385M had no effect on the VSV-induced expression of *Ifnb1* mRNA or replication of VSV (Fig. 3g and Supplementary Fig. 4h). We obtained similar results when we challenged cells with HSV-1 (Fig. 3h). Together these data suggested that MEKK2 dampened innate antiviral immunity in vitro, depending on its kinase activity.

MEKK2 deficiency potentiates the innate antiviral response in vivo. To investigate the role of MEKK2 in innate antiviral immunity more specifically, we prepared primary peritoneal macrophages from wild-type and MEKK2-deficient (*Map3k2*$^{-/-}$) mice. *Ifnb1* and its downstream response genes *Cxcl10* and *Isg15* were significantly upregulated in *Map3k2*$^{-/-}$ macrophages after stimulation with SeV or 5′-triphosphate RNA, relative to their expression in wild-type macrophages (Supplementary Fig. 5a,b). After challenge with VSV or HSV-1, *Ifnb1* expression and IFN-β secretion were much higher in *Map3k2*$^{-/-}$ macrophages than in wild-type macrophages (Fig. 4a,b and Supplementary Fig. 5c). In line with those findings, the copy number and replication of VSV or HSV-1 were much lower in *Map3k2*$^{-/-}$ macrophages than in wild-type macrophages (Fig. 4a,b). The abundance of the VSV-specific protein VSV-G was also lower in *Map3k2*$^{-/-}$ macrophages than in wild-type macrophages (Supplementary Fig. 5d). The expression of *Ifnb1* mRNA induced by SeV, 5′-triphosphate RNA, poly (I:C) or HSV-1, as well as that of the downstream genes *Cxcl10* and *Isg15*, was significantly upregulated in *Map3k2*$^{-/-}$ bone marrow–derived macrophages and MEFs relative to that in their wild-type counterparts (Supplementary Fig. 6a,b).

To investigate the function of MEKK2 in innate antiviral immunity in vivo, we challenged wild-type and *Map3k2*$^{-/-}$ mice with VSV. The expression of *Ifnb1* mRNA was significantly higher in the lungs, spleen and liver of *Map3k2*$^{-/-}$ mice than in those organs of wild-type mice (Fig. 4c). The concentration of IFN-β was also higher in the serum of *Map3k2*$^{-/-}$ mice than in that of wild-type mice (Fig. 4d). Consistent with increased production of IFN-β, the abundance of VSV-specific mRNA, the expression of VSV-G protein and VSV titers were lower in the lungs, liver and spleen of *Map3k2*$^{-/-}$ mice than in those organs of wild-type mice (Fig. 4e–g). Hematoxylin-and-eosin staining of the lungs after infection with VSV showed less infiltration of immune cells and less injury in *Map3k2*$^{-/-}$ mice than in wild-type mice (Fig. 4h). The innate antiviral response of wild-type and *Map3k2*$^{-/-}$ mice after challenge with HSV-1 was similar to that noted after infection with VSV (Fig. 4i–l). These in vivo results indicated that MEKK2 was an important negative regulator of innate antiviral immune responses to both an RNA virus and a DNA virus.

Host MEKK2 is required for TEX-induced innate immunosuppression. *Map3k2*$^{-/-}$ peritoneal macrophages showed enhanced SeV-induced dimerization of IRF3 relative to that of wild-type peritoneal macrophages but showed no difference in p-IRF3 or p-TBK1 (Fig. 5a). More notably, LLC cell–derived exosomes antagonized the dimerization of IRF3 in wild-type peritoneal macrophages but showed no inhibitory effect in the *Map3k2*$^{-/-}$ counterparts (Fig. 5a), which indicated that host MEKK2 was required for TEX-mediated antiviral immunosuppression. Consistent with that, *Ifnb1* expression induced by VSV or HSV-1 was repressed by LLC cell–derived exosomes in wild-type macrophages but not in *Map3k2*$^{-/-}$ macrophages (Fig. 5b,c). Accordingly, the titers of VSV and HSV-1 were increased by LLC cell–derived exosomes only in wild-type macrophages, relative to their titers in cells treated with MLF-derived (control) exosomes (Fig. 5b,c). To investigate the role of MEKK2 in TEX-mediated antiviral immunosuppression in vivo, we injected LLC cell–derived TEXs into the tail vein of wild-type and *Map3k2*$^{-/-}$ mice every other day for 3 weeks and challenged the mice with VSV or HSV-1. As expected, injection of LLC cell–derived TEXs into the mice led to a lower concentration of IFN-β in the serum of wild-type mice but not in the serum of *Map3k2*$^{-/-}$ mice (Fig. 5d,e). Furthermore, after pre-injection of LLC cell–derived TEXs, the titers of VSV and HSV-1 were increased in wild-type mice but not in *Map3k2*$^{-/-}$ mice (Fig. 5d,e). Moreover, LLC cell–derived TEXs substantially increased the sensitivity of wild-type mice to VSV or HSV-1,relative to the sensitivity of mice treated with MLF-derived (control) exosomes, but such a difference was not observed for *Map3k2*$^{-/-}$ mice (Fig. 5f). To confirm that MEKK2 was also required for the tumor cell–induced innate antiviral immunological defect, we inoculated wild-type and *Map3k2*$^{-/-}$ mice with LLC cells and assessed the innate antiviral immunity of these mice. After being challenged with VSV or HSV-1, wild-type mice inoculated with LLC cells showed much less IFN-β in the serum than that of the non-inoculated wild-type mice, whereas inoculation of *Map3k2*$^{-/-}$ mice with LLC cells did not obviously affect serum concentration of IFN-β (Fig. 5g). In line with those findings, the replication and viral titers of VSV and HSV-1 were increased in wild-type mice given LLC cell xenografts but not in their *Map3k2*$^{-/-}$ counterparts (Fig. 5h). These data indicated that these tumor cells and TEXs impaired host innate antiviral immunity via MEKK2.

MEKK2 interacts with IRF3 and interferes with its activation. We next sought to investigate the mechanism by which MEKK2 inhibited IFN-β signaling. Ectopic expression of wild-type MEKK2 suppressed the SeV-induced expression of *Ifnb1* mRNA in *MEKK2*-deficient cells, but ectopic expression of the mutant MEKK2 K385M did not (Fig. 6a). To determine which component of IFN-β signaling was affected by MEKK2, we ectopically expressed MEKK2 in HEK293T cells, or depleted HEK293T cells of MEKK2, together with the transfection of expression vectors for major components of the signaling pathway. Constitutively active IRF3 (IRF3-5D) mimics the virus-activated phosphorylated form of IRF3 in its ability to dimerize, translocate to the nucleus and activate the transcription of target genes in the absence of viral infection[33]. The activity of an IFN-β luciferase reporter and expression of *IFNB1* mRNA induced by the upstream active components (that the cells were transfected to express) were in all cases inhibited by ectopic expression of MEKK2 and upregulated by depleting cells of MEKK2 (Fig. 6b and Supplementary Fig. 7a), which suggested that MEKK2 affected IFN-β signaling at the level of IRF3. Moreover, ectopically expressed MEKK2 specifically interacted with IRF3 (Fig. 6c). MEKK2 was also found to co-immunoprecipitate with IRF3 in cells not transfected to ectopically express MEKK2 (Fig. 6d). We subsequently assessed the effect of MEKK2 on the activation of IRF3. After infection with SeV, the phosphorylation of TBK1, IKKε and IRF3 in wild-type macrophages was comparable to that in *Map3k2*$^{-/-}$ macrophages, but the formation of IRF3 dimers was greater in the *Map3k2*$^{-/-}$ cells (Fig. 6e). In HEK293T cells depleted of MEKK2, IRF3 dimerization was also enhanced (Supplementary Fig. 7b). In line with that finding, the ectopically expressed wild-type MEKK2 impaired SeV-induced dimerization of IRF3, but the ectopically expressed kinase-dead mutant MEKK2 K385M did not (Fig. 6f). Moreover, cells with ectopic-expression of wild-type MEKK2 showed severely impaired translocation of IRF3 to the nucleus after stimulation with SeV, whereas cells expressing MEKK2 K385M showed no such effect (Fig. 6g). Analysis of nuclear and cytoplasmic fractions revealed that the entry of IRF3 into the nucleus in response to SeV infection was greater in *Map3k2*$^{-/-}$ MEFs than in wild-type MEFs (Fig. 6h).

These results supported the conclusion that MEKK2 inhibited the dimerization of IRF3 and its translocation to the nucleus.

MEKK2 directly phosphorylates IRF3 at Ser173. Of note, wild-type MEKK2 induced a shift in the mobility of endogenous IRF3, as detected by SDS-PAGE, but the kinase-dead mutant MEKK2 K385M did not (Fig. 6f). Also, when ectopically expressed in HEK293T cells, only wild-type MEKK2, not MEKK2 K385M, induced a shift in the mobility of the co-expressed Myc-tagged IRF3 (Fig. 7a). Endogenous IRF3 in HEK293T cells also showed an obvious shift in mobility after overexpression of MEKK2; this shift disappeared after incubation of the cell lysates with λ-phosphatase (Fig. 7b). This indicated that MEKK2 directly or indirectly mediated the phosphorylation of IRF3, which then inhibited the activation of IRF3. Next we treated the cells with the MEK inhibitors U0126 or PD98059, the JNK inhibitor SP600125, the kinase p38 inhibitor SB203580, or the MEK5 and ERK5 inhibitors BIX02188 or BIX02189. However, none of these kinase inhibitors were able inhibit the shift in IRF3's mobility (Supplementary Fig. 7c), which suggested that MEKK2 was able to phosphorylate IRF3 directly. We next performed mass spectrometry of Flag-tagged IRF3 after overexpressing it in the presence or absence of MEKK2. This analysis identified IRF3 residues Ser173 and Ser175 as specific phosphorylation sites targeted by MEKK2 (Fig. 7c,d). We also checked IRF3 for residues with similar motifs and identified Thr180 and Ser188 as Ser173- and Ser175-related sites. We subsequently constructed a series of IRF3 point mutants in which one or more of these four residues was (were) replaced with alanine. Co-expression of each of those IRF3 mutants with wild-type MEKK2 or MEKK2 K385M showed that substitution of Ser173 almost completely blocked the shift in the mobility of IRF3 induced by MEKK2, whereas the other substitutions did not have obvious effects (Fig. 7e). This indicated that Ser173 was critical for the MEKK2-induced shift in the mobility of IRF3. To determine whether MEKK2 was indeed able to phosphorylate IRF3 Ser173 directly, we generated an antibody specific for the IRF3 Ser173-phosphorylation site. Use of this antibody showed that wild-type MEKK2 stimulated the phosphorylation of His-tagged wild-type IRF3 in vitro, whereas phosphorylation of a His-tagged IRF3 mutant with replacement of Ser173 with alanine (S173A) was not detected (Fig. 7f). In wild-type peritoneal macrophages, exosomes derived from $EGFR^+$ LLC cells triggered phosphorylation of IRF3 at Ser173, but exosomes from $EGFR^-$ LLC cells did not, whereas this phosphorylation was absent in *Map3k2*$^{-/-}$ cells (Fig. 7g); this confirmed that EGFR delivered via TEXs promoted MEKK2-dependent phosphorylation of IRF3 at Ser173.

MEKK2 promotes K33-linked poly-ubiquitination of IRF3. When we probed lysates of wild-type MEKK2 expressing cells with an antibody to IRF3, we observed trace amounts of high-molecular-weight proteins. A typical smear pattern was observed when these IRF3 immunoprecipitates were blotted for ubiquitin (Fig. 7h). Expression of MEKK2 K385M did not trigger this poly-ubiquitination of IRF3 (Fig. 7h), which indicated that the kinase activity of MEKK2 was required for this. The MEKK2-induced poly-ubiquitination of IRF3 seemed to be non-degradative, because after ectopic expression of MEKK2, the amount of both endogenous IRF3 and exogenous IRF3 remained unaffected (Fig. 7a,b). Furthermore, we found that ectopically expressed IRF3 was conjugated with multiple types of ubiquitin chains, but only Lys33 (K33)-linked poly-ubiquitination of IRF3 was upregulated by MEKK2 (Fig. 7i). Moreover, MEKK2 promoted K33-linked poly-ubiquitination of wild-type IRF3 but not of IRF3 S173A (Fig. 7i), which indicated that phosphorylation of IRF3 at Ser173 was required for the MEKK2 induced K33-linked poly-ubiquitination of IRF3. We next constructed a phosphorylation-mimicking mutant of IRF3 by replacing Ser173 with aspartic acid (S173D). Interestingly, basal K33-linked poly-ubiquitination was more abundant in this IRF3 S173D mutant than in wild-type IRF3 (Fig. 7j), which suggested that phosphorylation of IRF3 at Ser173 primed the K33-linked poly-ubiquitination of IRF3. Mass spectrometry of IRF3 revealed that Lys77, an undefined site within the nuclear localization signal (NLS)[34] of IRF3, was ubiquitinated after ectopic expression of MEKK2 (Fig. 7c). When Lys77 was replaced with arginine (K77R), the IRF3 S173D–induced K33-linked poly-ubiquitination of IRF3 became undetectable (Fig. 7j), which suggested that the K33-linked poly-ubiquitin was conjugated mainly to IRF3 Lys77.

Lys77 is located in the NLS of IRF3, which would indicate that the K33-linked poly-ubiquitin chain on Lys77 of IRF3 might affect the localization of IRF3 to the nucleus. Translocation of IRF3 to the nucleus relies on the classical nuclear import pathway that involves importin NLS receptors[35,36], We also found that wild-type MEKK2 inhibited the interaction between constitutively active IRF3-5D and importin α5 or β1, but MEKK2 K385M did not (Supplementary Fig. 7d). MEKK2 deficiency promoted the association between endogenous IRF3 and importin α5 or β1 after infection with SeV (Supplementary Fig. 7e). Moreover, IRF3 S173A showed increased association with importin α5 and β1 after infection with SeV, whereas the phosphorylation-mimicking mutant IRF3 S173D showed considerably decreased association (Fig. 7k). The reduced interaction with importin caused by the substitution in IRF3 S173D was 'rescued' by the K77R substitution (Supplementary Fig. 7f). In addition, $EGFR^+$ TEXs mitigated the association between IRF3 and importin α5 or β1 in wild-type MEFs but not in *Map3k2*$^{-/-}$ macrophages, after stimulation with SeV (Fig. 7l). Together these data revealed that TEX-activated MEKK2 was able to phosphorylate IRF3 on Ser173, which primed K33-linked poly-ubiquitination on Lys77 and thereby blocked the entry of IRF3 into the nucleus after viral stimulation (working model, Fig. 7k).

IRF3 S173A 'knock-in' restores innate antiviral immunity after TEX treatment. To understand the functional importance of the phosphorylation of IRF3 at Ser173 in innate immunity, we used the CRISPR-Cas9 system to create a knock-in (KI) mutation encoding S173A in both copies of *IRF3* in HEK293T cells and HeLa cells (called 'S173A-KI' here) (Fig. 8a). Homozygosity for this mutation encoding S173A was confirmed by Sanger sequencing (Fig. 8b). Immunoblot analysis with the antibody specific for IRF3 phosphorylated at Ser173 showed that overexpression of MEKK2 or treatment with TEXs indeed induced phosphorylation of endogenous IRF3 at Ser173 in the parental cells but not in the S173A-KI cells (Fig. 8c,d). Moreover, after infection with SeV, the dimerization of IRF3 was much more efficient in the S173A-KI cells than in the parental cells (Fig. 8e). Furthermore, MEKK2- or TEX-induced K33-linked poly-ubiquitination of endogenous IRF3 was observed only in the parental cells, not in the S173A-KI cells (Fig. 8f,g). Immunofluorescence analysis showed that MEKK2 also failed to impede the entry of IRF3 into the nucleus of S173A-KI cells after infection with SeV (Fig. 8h). This entry into the nucleus was also faster and more efficient in the S173A-KI cells than in the parental cells (Fig. 8i). We subsequently assessed *IFNB1* expression in the S173A-KI cells. *IFNB1* expression induced by SeV, VSV, cGAS plus STING, or poly(dA:dT) was much higher in the S173A-KI cells than in the parental cells (Fig. 8j). We next pre-treated S173A-KI cells and parental cells with exosomes and assessed the effect of this on SeV-induced *IFNB1* expression. In line with the experiments above, A549 cell–derived exosomes efficiently inhibited the SeV-induced *IFNB1* expression in the parental cells but did not significantly inhibit this in the S173A-KI cells (Fig. 8k). In conclusion, our study has demonstrated that MEKK2 inhibited the dimerization of IRF3 and its entry into the nucleus by phosphorylating IRF3 on Ser173, which was required for TEX-mediated suppression of host innate antiviral immunity (Supplementary Fig. 8e).

Discussion

Immunological defects can be caused by various conditions and diseases, including, for example, malignancy, organ or stem cell transplantation, systemic vasculitis, and connective tissue disease. In patients with lung cancer that had not undergone any procedures such as intramuscular injection or chemotherapy, we observed impaired induction of IFN-β in relative to its induction in patients who did not have cancer. We showed that tumor cells were able to repress host innate antiviral immunity by secreting and transferring EGFR$^+$ exosomes to innate immune cells. Active EGFR stimulated the host's MEKK2, which then phosphorylated IRF3 at Ser173; this led to repression of the activation of IRF3 and type I interferon and weakening of the host's pathogen-defense ability.

Activated EGFR recruits various cytoplasmic proteins that transduce and/or regulate its function. The EGFR pathway induces the proliferation, differentiation, migration, adhesion and survival of cells through various interacting signaling pathways, including RAS–RAF–MAPK, PI3K and JAK–STAT[37,38]. Cancer cells can transfer receptor tyrosine kinases such as phosphorylated EGFR and human EGFR2 (HER-2) to monocytes via exosomes, which prolongs monocyte survival and changes the microenvironment of cancers[39]. Here we demonstrated that multiple types of cancer cells secreted EGFR$^+$ exosomes. In addition, our results showed that cancer cells were able to deliver activated EGFR to macrophages, which interfered with the innate antiviral immunity via MEKK2-mediated deregulation of IRF3. Interestingly, we noticed in our in vitro analysis that EGFR$^-$ exosomes, as well as boiled tumor exosomes, reduced virus-induced expression of *IFNB1* in recipient macrophages slightly, which indicated that nucleic acids in tumor exosomes might also be suppressive in vitro. Since substantial EGFR-independent effects of tumor exosomes were not observed in vivo, we concluded that the TEX-derived EGFR had a major role in antagonizing innate antiviral immunity in the host.

MEKK2 is a serine-threonine kinase that belongs to the MEKK-STE11 subgroup of the MAP3K family of kinases. After upstream activation, MEKK2 can activate the ERK5 and JNK kinase pathways. Here we showed that MEKK2 mediated phosphorylation of IRF3 at Ser173 independently of ERK5 and JNK in cells in vivo and phosphorylated IRF3 at Ser173 directly in vitro. Furthermore, we found that, via phosphorylation of IRF3 at Ser173, MEKK2 inhibited the virus-induced translocation of IRF3 to the nucleus by triggering K33-linked poly-ubiquitination on the IRF3 NLS motif. Homozygous replacement of endogenous wild-type IRF3 with the mutant IRF3 S173A resulted in very low levels of K33-linked poly-ubiquitination of IRF3 after activation of MEKK2 or treatment with exosomes and increased the translocation of IRF3 to the nucleus and expression of *IFNB1* after viral stimulation. Interestingly, there was less expression of IFN-β in wild-type cells and mice than in their *Map3k2*$^{-/-}$ counterparts, even without addition of EGFR$^+$ TEXs, which would suggest that MEKK2 was (partially) active without stimulation via EGFR$^+$ TEXs, probably due to the induction of multiple cytokines and cellular stress pathways[30,31,40,41]. Whether and how such stimuli might regulate innate antiviral immunity via MEKK2 awaits further investigation.

It is known that two members of the IRF family, IRF3 and IRF7, can control the induction of interferons[42]. We found that the Ser173 motif of IRF3 was not conserved in IRF7. Consistent with that, only IRF3-mediated transcription was repressed by EGFR$^+$ exosomes and MEKK2. Published reports have demonstrated that IRF7, not IRF3, is responsible for the induction of IFN-α and IFN-β in plasmacytoid dendritic cells in response to viral infection[42–44], which therefore excludes the possibility of an effect of plasmacytoid dendritic cells on this TEX-mediated immunosuppression.

Emerging evidence shows that tumors can interfere with the immune system via secreted exosomes. By delivering different signals, TEXs can affect the proliferation, apoptosis, cytokine production and reprogramming of T cells[27,45,46]. TEXs also downregulate expression of the stimulatory receptor NKG2D and reduce the cytotoxicity of natural killer cells[47]. In addition, TEXs can inhibit the differentiation of monocytes into dendritic cells and cytotoxic T lymphocytes and can skew the differentiation of myeloid precursor cells into myeloid-derived suppressor cells[48,49]. Here we have described how cancer cells managed to regulate host innate antiviral immunity. Moreover, by elucidating a novel TEX-mediated control mechanism of IRF3 signaling in recipient macrophages, we have revealed, for the first time, to our knowledge, previously unknown interplay between tumor cells and antiviral innate immunity of the host, in which MEKK2 is the first host kinase identified, to our knowledge. We have also, for the first time, to our knowledge, shown how phosphorylation of IRF3 at Ser173 and subsequent K33-linked poly-ubiquitination regulated the function of IRF3. These mechanistic studies might explain the diminished innate antiviral immunity frequently found in patients with cancer[50].

Methods

Methods, including statements of data availability and any associated accession codes and references, are available at https://doi.org/10.1038/s41590-017-0043-5.

Received: 1 June 2017; Accepted: 20 December 2017;
Published online: 22 January 2018

References

1. Wu, J. & Chen, Z. J. Innate immune sensing and signaling of cytosolic nucleic acids. *Annu. Rev. Immunol.* **32**, 461–488 (2014).
2. Kato, H., Takahasi, K. & Fujita, T. RIG-I-like receptors: cytoplasmic sensors for non-self RNA. *Immunol. Rev.* **243**, 91–98 (2011).
3. Alexopoulou, L., Holt, A. C., Medzhitov, R. & Flavell, R. A. Recognition of double-stranded RNA and activation of NF- κB by Toll-like receptor 3. *Nature* **413**, 732–738 (2001).
4. Yoneyama, M. et al. The RNA helicase RIG-I has an essential function in double-stranded RNA-induced innate antiviral responses. *Nat. Immunol.* **5**, 730–737 (2004).
5. Pichlmair, A. et al. RIG-I-mediated antiviral responses to single-stranded RNA bearing 5′-phosphates. *Science* **314**, 997–1001 (2006).
6. Hornung, V. et al. 5′-Triphosphate RNA is the ligand for RIG-I. *Science* **314**, 994–997 (2006).
7. Kato, H. et al. Differential roles of MDA5 and RIG-I helicases in the recognition of RNA viruses. *Nature* **441**, 101–105 (2006).
8. Sun, L., Wu, J., Du, F., Chen, X. & Chen, Z. J. Cyclic GMP-AMP synthase is a cytosolic DNA sensor that activates the type I interferon pathway. *Science* **339**, 786–791 (2013).
9. Unterholzner, L. et al. IFI16 is an innate immune sensor for intracellular DNA. *Nat. Immunol.* **11**, 997–1004 (2010).
10. Sato, S. et al. Toll/IL-1 receptor domain-containing adaptor inducing IFN-β (TRIF) associates with TNF receptor-associated factor 6 and TANK-binding kinase 1, and activates two distinct transcription factors, NF-κB and IFN-regulatory factor-3, in the Toll-like receptor signaling. *J. Immunol.* **171**, 4304–4310 (2003).
11. Seth, R. B., Sun, L., Ea, C. K. & Chen, Z. J. Identification and characterization of MAVS, a mitochondrial antiviral signaling protein that activates NF-κB and IRF 3. *Cell* **122**, 669–682 (2005).
12. Ishikawa, H. & Barber, G. N. STING is an endoplasmic reticulum adaptor that facilitates innate immune signalling. *Nature* **455**, 674–678 (2008).
13. Takeuchi, O. & Akira, S. Pattern recognition receptors and inflammation. *Cell* **140**, 805–820 (2010).
14. Kawai, T. & Akira, S. The role of pattern-recognition receptors in innate immunity: update on Toll-like receptors. *Nat. Immunol.* **11**, 373–384 (2010).
15. Takeuchi, O. & Akira, S. Innate immunity to virus infection. *Immunol. Rev.* **227**, 75–86 (2009).
16. Théry, C., Zitvogel, L. & Amigorena, S. Exosomes: composition, biogenesis and function. *Nat. Rev. Immunol.* **2**, 569–579 (2002).
17. Colombo, M., Raposo, G. & Théry, C. Biogenesis, secretion, and intercellular interactions of exosomes and other extracellular vesicles. *Annu. Rev. Cell. Dev. Biol.* **30**, 255–289 (2014).
18. Cocucci, E., Racchetti, G. & Meldolesi, J. Shedding microvesicles: artefacts no more. *Trends Cell. Biol.* **19**, 43–51 (2009).
19. Melo, S. A. et al. Cancer exosomes perform cell-independent microRNA biogenesis and promote tumorigenesis. *Cancer Cell.* **26**, 707–721 (2014).

20. Thakur, B. K. et al. Double-stranded DNA in exosomes: a novel biomarker in cancer detection. *Cell. Res.* **24**, 766–769 (2014).
21. Valadi, H. et al. Exosome-mediated transfer of mRNAs and microRNAs is a novel mechanism of genetic exchange between cells. *Nat. Cell. Biol.* **9**, 654–659 (2007).
22. Peinado, H. et al. Melanoma exosomes educate bone marrow progenitor cells toward a pro-metastatic phenotype through MET. *Nat. Med.* **18**, 883–891 (2012).
23. Benito-Martin, A., Di Giannatale, A., Ceder, S. & Peinado, H. The new deal: a potential role for secreted vesicles in innate immunity and tumor progression. *Front. Immunol.* **6**, 66 (2015).
24. Hoshino, A. et al. Tumour exosome integrins determine organotropic metastasis. *Nature* **527**, 329–335 (2015).
25. Melo, S. A. et al. Glypican-1 identifies cancer exosomes and detects early pancreatic cancer. *Nature* **523**, 177–182 (2015).
26. Robbins, P. D. & Morelli, A. E. Regulation of immune responses by extracellular vesicles. *Nat. Rev. Immunol.* **14**, 195–208 (2014).
27. Whiteside, T. L. Exosomes and tumor-mediated immune suppression. *J. Clin. Invest.* **126**, 1216–1223 (2016).
28. Théry, C., Ostrowski, M. & Segura, E. Membrane vesicles as conveyors of immune responses. *Nat. Rev. Immunol.* **9**, 581–593 (2009).
29. Cheng, J. et al. Mip1, an MEKK2-interacting protein, controls MEKK2 dimerization and activation. *Mol. Cell. Biol.* **25**, 5955–5964 (2005).
30. Sun, W. et al. MEK kinase 2 and the adaptor protein Lad regulate extracellular signal-regulated kinase 5 activation by epidermal growth factor via Src. *Mol. Cell. Biol.* **23**, 2298–2308 (2003).
31. Fanger, G. R., Johnson, N. L. & Johnson, G. L. MEK kinases are regulated by EGF and selectively interact with Rac/Cdc42. *EMBO J.* **16**, 4961–4972 (1997).
32. Cheng, J. et al. Dimerization through the catalytic domain is essential for MEKK2 activation. *J. Biol. Chem.* **280**, 13477–13482 (2005).
33. Lin, R., Mamane, Y. & Hiscott, J. Structural and functional analysis of interferon regulatory factor 3: localization of the transactivation and autoinhibitory domains. *Mol. Cell. Biol.* **19**, 2465–2474 (1999).
34. Zhu, M., Fang, T., Li, S., Meng, K. & Guo, D. Bipartite nuclear localization signal controls nuclear import and DNA-binding activity of IFN regulatory factor 3. *J. Immunol.* **195**, 289–297 (2015).
35. Kutay, U., Izaurralde, E., Bischoff, F. R., Mattaj, I. W. & Görlich, D. Dominant-negative mutants of importin-β block multiple pathways of import and export through the nuclear pore complex. *EMBO J.* **16**, 1153–1163 (1997).
36. Marfori, M. et al. Molecular basis for specificity of nuclear import and prediction of nuclear localization. *Biochim. Biophys. Acta* **1813**, 1562–1577 (2011).
37. Yarden, Y. & Pines, G. The ERBB network: at last, cancer therapy meets systems biology. *Nat. Rev. Cancer* **12**, 553–563 (2012).
38. Arteaga, C. L. & Engelman, J. A. ERBB receptors: from oncogene discovery to basic science to mechanism-based cancer therapeutics. *Cancer Cell.* **25**, 282–303 (2014).
39. Song, X. et al. Cancer cell-derived exosomes induce mitogen-activated protein kinase-dependent monocyte survival by transport of functional receptor tyrosine kinases. *J. Biol. Chem.* **291**, 8453–8464 (2016).
40. Kesavan, K. et al. MEKK2 regulates the coordinate activation of ERK5 and JNK in response to FGF-2 in fibroblasts. *J. Cell. Physiol.* **199**, 140–148 (2004).
41. Zhang, D. et al. Identification of MEKK2/3 serine phosphorylation site targeted by the Toll-like receptor and stress pathways. *EMBO J.* **25**, 97–107 (2006).
42. Marié, I., Durbin, J. E. & Levy, D. E. Differential viral induction of distinct interferon-α genes by positive feedback through interferon regulatory factor-7. *EMBO J.* **17**, 6660–6669 (1998).
43. Sato, M. et al. Distinct and essential roles of transcription factors IRF-3 and IRF-7 in response to viruses for IFN-α/β gene induction. *Immunity* **13**, 539–548 (2000).
44. Honda, K. et al. IRF-7 is the master regulator of type-I interferon-dependent immune responses. *Nature* **434**, 772–777 (2005).
45. Wieckowski, E. U. et al. Tumor-derived microvesicles promote regulatory T cell expansion and induce apoptosis in tumor-reactive activated $CD8^+$ T lymphocytes. *J. Immunol.* **183**, 3720–3730 (2009).
46. Whiteside, T. L. Immune modulation of T-cell and NK (natural killer) cell activities by TEXs (tumour-derived exosomes). *Biochem. Soc. Trans.* **41**, 245–251 (2013).
47. Szczepanski, M. J., Szajnik, M., Welsh, A., Whiteside, T. L. & Boyiadzis, M. Blast-derived microvesicles in sera from patients with acute myeloid leukemia suppress natural killer cell function via membrane-associated transforming growth factor-β1. *Haematologica* **96**, 1302–1309 (2011).
48. Valenti, R. et al. Tumor-released microvesicles as vehicles of immunosuppression. *Cancer Res.* **67**, 2912–2915 (2007).
49. Liu, Y. et al. Contribution of MyD88 to the tumor exosome-mediated induction of myeloid derived suppressor cells. *Am. J. Pathol.* **176**, 2490–2499 (2010).
50. Chemaly, R. F. et al. A multicenter study of pandemic influenza A (H1N1) infection in patients with solid tumors in 3 countries: early therapy improves outcomes. *Cancer* **118**, 4627–4633 (2012).

Acknowledgements

We thank B. Su (Yale University School of Medicine) for *Map3k2*$^{+/-}$ mice; and M. Rabeling (Leiden University Medical Center) for shRNA constructs. Supported by the special program from the Ministry of Science and Technology of China (2016YFA0502500 to L.Z.), the Chinese National Natural Science Funds (31701232 to F. X., 31571460 to F. Z., 31471315, 31671457, 31741086 and 91753139 to L.Z.), Jiangsu National Science Foundation (BK20150354 to F.Z.) and Zhejiang outstanding youth fund (LR14C070001 to L.Z.).

Author contributions

L.G., F.Z. and L.Z. designed the experiments and analyzed the data; L.G., L.W., T.D., K.J., Z.Z., S.W., F.X. and P.F. performed the experiments; B.Y. and H.H. contributed to writing and discussions and agree with the conclusion presented in the manuscript; and L.Z., H.v.D. and F.Z. wrote the manuscript.

Competing interests

The authors declare no competing financial interests.

Additional information

Supplementary information accompanies this paper at https://doi.org/10.1038/s41590-017-0043-5.

Reprints and permissions information is available at www.nature.com/reprints.

Correspondence and requests for materials should be addressed to F.Z. or L.Z.

Methods

Patients. The Second Affiliated Hospital of ChongQing Medical University Research Ethics Committee and the Ethics Committee approved the study, and written informed consent was obtained from all subjects. Nine patients with lung cancer (40–59 years age, mean = 53 years) and thirteen patients without cancer (40–62 years age, mean = 55 years), all with confirmed infection with influenza virus at Chonqing Medical University, were selected. Infection with influenza virus was confirmed by a Directigen FluA Kit. Samples were collected after informed consent was obtained. Serum samples were collected during the first to third febrile day. None of the patients had undergone any procedures, such as intramuscular injection. None of the patients with lung cancer had undergone chemotherapy. Serum samples were separated into aliquots and were stored at −80 °C until required for tanalysis.

Mice. *Map3k2*$^{+/-}$ mice were provided by B. Su and were self-crossed to generate *Map3k2*$^{-/-}$ mice and littermates[51,52]. Wild type mice were purchased from Shanghai SLAC Laboratory Animal. All mice were on the C57BL/6 J background and were maintained under specific-pathogen-free conditions in the animal facility of Soochow University. The Institutional Committee for Animal Welfare of the Soochow University approved this study.

Exosome isolation and treatment. Cells were cultured in Dulbecco's modified Eagle's medium (DMEM) supplemented with 10% FBS (FBS) depleted of exosomes. The culture medium was then harvested and subjected to sequential centrifugation steps (300 × *g* for 5 min; 2,000 × *g* for 15 min) to remove floating and dead cells. The supernatants were further concentrated by 100 K NMWL centrifugal filtration (Amicon Ultra-15, Millipore) and washed twice with 1× PBS before centrifuging at 10,000 × *g* for 90 min. Exosomes were recovered from the cleared, condensed supernatant by ultracentrifugation at 100,000 × *g* for 17 h at 4 °C. Exosome preparations were verified by electron microscopy. Exosome size and particle number were analyzed using the NS300 nanoparticle characterization system (NanoSight, Malvern Instruments).

Exosome pellets were resuspended in ice-cold 1× PBS and stored at 4 °C. The concentration of exosomal proteins was quantified by BCA Protein Assay Kit (Thermo Scientific). For 'education' experiments, mice received 50 μg of exosomes via the tail vein every other day for 3 weeks. To confirm exosome uptake by specific organs or cell types, labeled exosomes were injected 24 h before tissue collection and tissues were analyzed for exosome-positive cells by immunofluorescence or through bioluminescent imaging with the IVIS 100 (Caliper Life Sciences, Hopkinton, MA, USA).

Isolation of mouse embryonic fibroblast s (MEF s), macrophages and bone marrow–derived macrophages. Primary MEFs were prepared from the wild-type and *Map3k2*$^{-/-}$ embryos at day 15 and were cultured in Dulbecco's modified Eagle's medium (DMEM) supplemented with 10% FBS. Bone marrow–derived macrophages were isolated from the tibia and femur. Cells were cultured in DMEM with 10% FBS, glutamine and 30% L929 supernatant at 37 °C for 7 d. Peritoneal macrophages were harvested from mice 4 d after thioglycollate (BD) injection and cultured in DMEM supplemented with 5% FBS.

Cells and reagents. RAW264.7 cells, HEK293T cells, A549 cells, LLC cells, HeLa cells and MEFs were cultured at 37 °C under 5% CO_2 in DMEM supplemented with 10% FBS, 100 U/ml penicillin and 100 μg/ml streptomycin. THP-1 cells were cultured in RPMI 1640 supplemented with 10% FBS. All cell lines tested are negative for mycoplasma contamination. MG132 was bought from SelleckChem; poly(I:C) and 5′-triphosphate RNA were from Invivogen; λ-PPase was from Santa Cruz Biotechnology; Lapatinib, U0126 and PD98059 were from MedChem Express; and SP600125, SB203580, BIX02188, BIX02189 and the anti-cancer component library were from SelleckChem.

Nanoparticle tracking analysis. Suspensions containing vesicles were analyzed using NanoSight NS300 instruments (Malvern Instruments, Amesbury, UK). For this analysis, a monochromatic laser beam at 405 nm was applied to the dilute suspension of vesicles (0.22 μM filtered) with a concentration within the recommended measurement range (1×10^6 to 10×10^8 particles/ml). The Nanoparticle tracking analysis (NTA) software is optimized to first identify and then track each particle on a frame-by-frame basis; the Brownian movement of each particle is tracked and measured from frame to frame. The velocity of particle movement is used to calculate particle size by applyication of the two-dimensional Stokes-Einstein equation. NTA post-acquisition settings were optimized and kept constant between samples, and each video was then analyzed to give the mean, mode, and median vesicle size together with an estimate of the concentration.

Flow cytometry. For analysis of exosomes, 20 μg exosomes were mixed with 5 μl 4 μm aldehyde-sulfate latex beads (Invitrogen, lot:1743119) in 500 μl 1× PBS for 30 min at room temperature with continuous rotation. Exosome-bound beads were incubated with 1 μg anti-EGFR (#555997,BD Biosciences) for 30 min. The percentage of positive beads was calculated relative to the total number of beads analyzed per sample (10,000 events). This percentage was thereafter called the frequency of beads with EGFR$^+$ exosomes.

For cell analysis, 10,000 RAW264.7 cells were mixed with 1 μg PE-conjugated antibody to EGFR (#555997,BD Biosciences) in 500 μl DMEM for 30 min at 4 °C with continuous rotation. The frequency of EGFR$^+$ cells was calculated relative to the total number of cells analyzed per sample (10,000 events).

Stained exosomes or cells were analyzed on a Beckman CytoFlex using CytExpert software.

Plasmids and transfection. Expression plasmids encoding cGAS, RIG-IN, STING, IRF3-5D, MAVS, TBK1, IKKε and the plasmids IFNB1-Luc, ISRE-Luc and lentiCRISPRv2 were purchased from Addgene. MEKK2 was amplified by standard PCR and cloned in pLV-HA and pLV-Flag vector. Point mutations were generated by site-directed mutagenesis with KOD plus polymerase (Toyobo); plasmids encoding the wild-type protein were used as the template. All constructs were confirmed by DNA sequencing. For transient transfections of plasmids into HEK293T cells, standard calcium phosphate precipitation was used. For macrophages and THP-1 cells, the Geneporter 2 Transfection Reagent (Genlantis) was used for transfection. shRNAs were obtained from the Sigma Mission Library. We used TRCN00000382082 for mouse Rab27a, and TRCN0000279985 for human Rab27a; TRCN0000055218 for mouse EGFR was subcloned into Tet-pLKO-puro (#21915, Addgene) for doxycycline-inducible knockdown. sh*MAP3K2* was constructed in the pLKO.1 plasmid with following primers: sh-MAP3K2 #1 forward, 5′-CCGGGAATGATGTCCGAGTCAAATTCTCGAGAATTTGACTCGGACATCATTCTTTTTG-3′, and sh-MAP3K2 #1 reverse, 5′-AATTCAAAAAGAATGATGTCCGAGTCAAATTCTCGAGAATTTGACTCGGACATCATTC-3′; and sh-MAP3K2 #2 forward, 5′-CCGGAGTATGATGATAGTCGAATAACTCGAGTTATTCGACTATCATCATACTTTTTTG-3′, and sh-MAP3K2 #2 reverse, 5′-AATTCAAAAAAGTATGATGATAGTCGAATAACTCGAGTTATTCGACTATCATCATACT-3′.

Enzyme-linked immunosorbent assay (ELISA). The concentration of IFN-β in culture supernatants and serum was measured by ELISA Kits (R&D Systems).

Native PAGE (PAGE). Cells were lysed in RIPA lysis buffer (50 mM Tris-HCl, pH 7.4, 150 mM NaCl, 1% NP-40 and 100 μM PMSF) and 15 μg supernatant of total cell lysate (TCL) was separated by native PAGE after centrifugation. 7.5% native PAGE gels were made without SDS. Gels were pre-run with 25 mM Tris and 192 mM glycine, pH 8.4, with 1% deoxycholate (DOC) in a cathode chamber for 30 min at 40 mA. Samples in native sample buffer (10 μg protein, 62.5 mM Tris-Cl, pH 6.8, 15% glycerol and 1% DOC) were size fractionated by electrophoresis for 60 min at 25 mA and were transferred to PVDF membranes for immunoblot analysis.

Real-time quantitative RT-PCR (qRT-PCR). Total RNA was prepared using the NucleoSpin RNA II kit (BIOKÉ, Netherlands). A total of 1 μg of RNA was reverse-transcribed using the RevertAid First Strand cDNA Synthesis Kit (Fermentas). Real-time PCR was conducted with SYBR Green (Applied Bioscience) using a StepOne Plus real-time PCR system (Applied Bioscience). Quantitation of all target-gene expression was normalized to *Gapdh* for mouse genes or *GAPDH* for human genes. qPCR primers were as follows:

Murine *Ifnb1* forward: 5′-TCCTGCTGTGCTTCTCCACCACA-3′;
Murine *Ifnb1* reverse: 5′-AAGTCCGCCCTGTAGGTGAGGTT-3′;
Murine *Cxcl10* forward: 5′-ATCATCCCTGCGAGCCTATCCT-3′;
Murine *Cxcl10* reverse: 5′-GGCCTGGGACCTAAAGGTGAAGA-3′;
Murine *Isg15* forward: 5′-AAAGGGTAAGACCGTCCTGGAGC-3′;
Murine *Isg15* reverse: 5′-TTGGCACACACTTGGCGGTTC-3′;
Murine *Gapdh* forward: 5′-GGCCTTCCGTGTTCCTACC-3′;
Murine *Gapdh* reverse: 5′-AGCCCAAGATGCCCTTCAGT-3′;
VSV forward: 5′-ACGGCGTACTTCCAGATGG-3′;
VSV Reverse: 5′-CTCGGTTCAAGATCCAGGT-3′;
HSV-1 genomic DNA forward: 5′-TGGGACACATGCCTTCTTGG-3′;
HSV-1 genomic DNA reverse: 5′
-ACCCTTAGTCAGACTCTGTTACTTACCC-3′;
Human *IFNB1* forward: 5′- CCAACAAGTGTCTCCTCCAAAT-3′;
Human *IFNB1* reverse: 5′-AATCTCCTCAGGGATGTCAAAGT-3′;
Human *GAPDH* forward: 5′- AGGGCTGCTTTTAACTCTGGT-3′;
Human *GAPDH* reverse: 5′- CCCCACTTGATTTTGGAGGGA-3′.

CRISPR-Cas9–mediated genome editing. CRISPR-Cas9 genomic editing for gene deletion or replacement was used as previously described[53]. For deletion of the gene encoding EGFR, two CRISPR small guide RNAs (sgRNAs) were cloned into the vector lentiCRISPRv2 (addgene) and transfected into LLC cells. 48 h after transfection, cells were placed under puromycin selection for 1 week, then single clones were picked, grown and identified by immunoblot analysis and sequencing. The guide RNA sequences that were used were as follows: EGFR sg set1, 5′-CACCGGGATAGTATCCATATTGCAG-3′; and EGFR sg set2, 5′-AAACCTGCAATATGGATACTATCCC-3′.

To create IRF3-S173A gene-targeted alleles in human cells, two sgRNA sequences near the codon encoding Ser173 were chosen on the basis of their specificity scores (http://crispr.mit.edu/). The sgRNA sequences were then cloned into the lentiCRISPRv2 plasmid. The repair template harboring ~1-kb homology arms flanking the IRF3 S173 codon was amplified from the genomic DNA of human cells and cloned into pcDNA3.1 plasmid. The mutation encoding S173A (AGC → GCC) was then introduced into the repair template. To avoid the cleavage of the repair template by Cas9, additional synonymous mutation was designed to make the repair template sequence different from the sgRNA sequences. The lentiCRISPRv2 plasmids and repair template were co-transfected into HEK293T cells and HeLa cells. 48 h later, the cells were treated with 2 μg/mL puromycin for 3 d to remove the cells without transfection, and subsequently, single cells were seeded into separate wells of 96-well plates. After clonal expansion, genomic DNA was amplified by PCR using primers flanking IRF3 S173 codon. The PCR products were then sequenced to validate the IRF3 S173A mutation in both alleles.

The sgRNA sequences were as follows: IRF3 S173 sg set1, 5′ - TGTCCAAGCTGGGGCTCCGC-3′; and IRF3 S173 sg set 2, 5′-GGGAGTGGGATTGTCCAAGC-3′;

The primer sequences that introduce the S173A and synonymous mutation to repair template were as follows: IRF3MF: 5′ -CCTGCGGGCCCCATCCTTGGACAATCCCACTCCCTTCCC-3′; and IRF3MR: 5′-GTCCAAGGATGGGGCCCGCAGGGGCTGAGGGCA-3′.

Immunoprecipitation and immunoblot analysis. Cells were lysed with 1 ml lysis buffer (20 mM Tris-HCl, pH 7.4, 2 mM EDTA, 25 mM NaF and 1% Triton X-100) containing protease inhibitors (Sigma) for 10 min at 4 °C. After centrifugation at 12,000 × *g* for 15 min, the protein concentrations were measured, and equal amounts of lysates were used for immunoprecipitation. Immunoprecipitation was performed with anti-FLAG M2 beads (Sigma, A2220) for 1 h at 4 °C or with different antibodies and protein A-Sepharose (GE Healthcare Bio-Sciences AB) for 3 h at 4 °C. Thereafter, the precipitants were washed three times with washing buffer (50 mM Tris-HCl, pH 8.0, 150 mM NaCl, 1% Nonidet P-40, 0.5% sodium deoxycholate and 0.1% SDS), and the immunocomplexes were eluted with sample buffer containing 1% SDS for 5 min at 95 °C. The immunoprecipitated proteins were thereafter separated by SDS-PAGE. Immunoblot analysis was performed with specific antibodies and secondary anti-mouse or anti-rabbit conjugated to horseradish peroxidase (Amersham Biosciences). Visualization was achieved with chemiluminescence.

Antibodies used for immunoprecipitation (IP), immunoblotting (IB) and immunofluorescence (IF) were as follows: anti-EGFR a (#4267S, Cell Signaling, 1:1,000 for IB), anti-EGFR antibody (ab231, Abcam, 1:1,000 for IB), antibody to EGFR phosphorylated at Tyr1068 (#3777S, Cell Signaling, 1:1,000 for IB), anti-MEKK2 (ab33918, Abcam, 1:1,000 for IB), anti-Flag (M2, Sigma, 1:5,000 for IB), anti-HA (Y-11, sc-805, Santa Cruz Biotechnology, 1:1,000 for IB and 1:200 for IF), anti-Myc (a-14, sc-789, Santa Cruz Biotechnology, 1:1,000 for IB), rabbit monoclonal antibody (mAb) to IRF3 (#11904, Cell Signaling, 1:1,000 for IB and 1:200 for IF), rabbit mAb to IRF3 phosphorylated at Ser396 (#4947, Cell Signaling, 1:1,000 for IB), rabbit mAb to TBK1 (#3504, Cell Signaling, 1:1,000 for IB), rabbit mAb to TBK1 phosphorylated at Ser172 (#5483, Cell Signaling, 1:1,000 for IB), anti-importin α5 (18137-1-AP, Proteintech, 1:1,000 for IB), anti-importin β1 (#51186, Cell Signaling, 1:1,000 for IB) and anti-VSV-G (ABGENT, AP1016a, 1:1,000 for IB). Secondary HRP-conjugated anti-mouse (NA931) or anti-rabbit (NA934) (Amersham Biosciences, 1:10,000 for IB), secondary AlexaFluor488-labeled anti-rabbit (Molecular Probes R37116, 1:300 for IF) or AlexaFluor593-labeled anti-mouse (Molecular Probes R3712, 1:300 for IF) were used. The polyclonal antibody to IRF3 phosphorylated at Ser173 was generated by GL Biochem (Shanghai) by immunizing rabbits with Cys-PQPLRp(S) PSLDNPT peptide.

Protein purification. His-IRF3 wild-type and His-IRF3 S173A mutant constructs were generated by sub-cloning into pET-28a. His-IRF3 plasmids were used to transform the *Escherichia coli* strain BL21. Cultures were grown overnight at 37 °C. The next day, cultures were diluted 1:50 in fresh LB medium and were grown at 37 °C to an OD600 of 0.6. Cells were then induced overnight at 24 °C in the presence of 0.5 mM isopropyl-β-D-thiogalactopyranoside (IPTG), 20 mM HEPES, pH 7.5, 1 mM $MgCl_2$ and 0.05% glucose. For His-IRF3 purification, the washed cell pellet was resuspended in lysis buffer (50 mM HEPES-KOH, pH 7.6, 500 mM NaCl, 25 mM $MgCl_2$, 20% glycerol, 0.1% NP-40, complete EDTA free protease inhibitors (Roche) and 1 mM PMSF). After sonication and a freeze–thaw step, the supernatant of the cell lysate was incubated with Talon beads (BD Biosciences) in the presence of 20 mM imidazole. Beads were washed four times with lysis buffer lacking imidazole. Purified proteins were eluted in lysis buffer containing 200 mM imidazole. For the purification of MEKK2 wild-type and MEKK2 (K385M) protein from mammalian cells, Flag-MEKK2 wild-type or MEKK2 (K385M) expression plasmids were transfected in HEK293T cells and Flag-MEKK2 wild-type or MEKK2 (K385M) protein were immunoprecipitated overnight from the cell lysate with a-Flag-M2 resin (Sigma), followed by elution with Flag peptide (Sigma, 1 mg/ml in 50 mM HEPES, pH 7.5, 100 mM NaCl, 0.1% NP40 and 5% glycerol).

Transcription reporter assay. HEK293T cells were seeded in 24-well plates, transfected with the indicated plasmids using the calcium phosphate method and subsequently (mock) treated and harvested at indicated time points. The internal transfection control *renilla* was used to normalize the luciferase activities for differences in transfection efficiency.

Lung histology. Lungs from control or virus-infected mice were dissected, fixed in 10% phosphate-buffered formalin, embedded into paraffin, sectioned, stained with hematoxylin and eosin solution, and examined by light microscopy for histological changes.

Immunofluorescence and confocal microscopy. HeLa cells grown on glass coverslips were transfected with plasmids and infected with or without SeV as indicated. Cells were then washed with PBS and fixed with 4% paraformaldehyde in PBS for 20 min, permeabilized with 0.2% Triton X-100 and blocked with 3% bovine serum albumin. Then the cells were stained with indicated antibodies (identified above), followed by incubation with fluorescent-dye-conjugated secondary antibodies (identified above). Nuclei were counterstained with DAPI (Sigma-Aldrich).

Viral infection and plaque assay. Mouse macrophages or other cells (2×10^5) were plated 24 h before infection. Cells were infected with VSV (0.1 MOI), HSV-1 (10 MOI) or SeV (100 hemagglutination units [HAU]/ml) for the indicated times. VSV plaque assay and VSV replication were determined by a standard $TCID_{50}$ assay on permissive Vero cell monolayers in 96-well plates with a series of tenfold-diluted samples. After 1 h infection, the plates were incubated for 48 h. The medium was then removed and the cells were fixed with 4% paraformaldehyde for 15 min and stained with 1% crystal violet for 30 min before plaque counting.

Viral infection in vivo. For in vivo viral infection studies, 8-week-old control and mutant mice were given intraperitoneal injection of VSV (5×10^8 pfu/mouse) or intranasal administration of HSV-1 (2×10^7 PFU per mouse). 24 h after infection, we collected the blood from mice orbit for ELISA and obtained the lungs, spleen and liver from the mice for RNA, protein and virus titer analysis. To measure the VSV titers in the lung, spleen and liver, and HSV-1 titers in the brain, snap-frozen tissues were weighed and homogenized three times (5 s each) in MEM. After homogenization, the suspensions were centrifuged at 1,620 *g* for 30 min, and the supernatants were used for plaque assays on monolayers of Vero cells seeded in 96-well plates with a series of tenfold-diluted samples. For the survival experiments, mice were monitored for survival after infection with VSV or HSV-1. For the induced model, doxycycline was administered to mice at indicated time point after injection of the cancer cells, through the diet (625 mg of food per kg body weight) as well as by intraperitoneal injection (25 mg per of body weight; two times per day).

Statistical analysis. Statistical analyses were performed with a two-tailed unpaired *t*-test or as indicated in the legends. *P* values are indicated by asterisks in the figures: * $P < 0.05$. Differences at $P = 0.05$ and lower were considered significant. For mouse survival studies, Kaplan–Meier survival curves were generated and analyzed for statistical significance with GraphPad Prism 5.0. Pilot studies were used for estimation of the sample size to ensure adequate power. There was no exclusion of data points or mice. No randomization or blinding was used.

Life Sciences Reporting Summary. Further information on experimental design and reagents is available in the Life Sciences Reporting Summary.

Data availability. The data that support the findings of this study are available from the corresponding author upon request.

References

51. Guo, Z. et al. Disruption of Mekk2 in mice reveals an unexpected role for MEKK2 in modulating T-cell receptor signal transduction. *Mol. Cell. Biol.* **22**, 5761–5768 (2002).
52. Chang, X. et al. The kinases MEKK2 and MEKK3 regulate transforming growth factor-β-mediated helper T cell differentiation. *Immunity* **34**, 201–212 (2011).
53. Ran, F. A. et al. Genome engineering using the CRISPR-Cas9 system. *Nat. Protoc.* **8**, 2281–2308 (2013).

nature research

Corresponding author(s): Fangfang Zhou, Long Zhang

☐ Initial submission ☐ Revised version ☒ Final submission

Life Sciences Reporting Summary

Nature Research wishes to improve the reproducibility of the work that we publish. This form is intended for publication with all accepted life science papers and provides structure for consistency and transparency in reporting. Every life science submission will use this form; some list items might not apply to an individual manuscript, but all fields must be completed for clarity.

For further information on the points included in this form, see Reporting Life Sciences Research. For further information on Nature Research policies, including our data availability policy, see Authors & Referees and the Editorial Policy Checklist.

Experimental design

1. Sample size

Describe how sample size was determined.

Sample size was determined according to different experimental aims. The number of independent experiment an technical replicates was indicated in each figure legend.

2. Data exclusions

Describe any data exclusions.

No data were excluded.

3. Replication

Describe whether the experimental findings were reliably reproduced.

All the findings were reliably reproduced.

4. Randomization

Describe how samples/organisms/participants were allocated into experimental groups.

Animals used were littermates allocated to groups on the base of their genotype.

5. Blinding

Describe whether the investigators were blinded to group allocation during data collection and/or analysis.

No blinding was used.

Note: all studies involving animals and/or human research participants must disclose whether blinding and randomization were used.

6. Statistical parameters

For all figures and tables that use statistical methods, confirm that the following items are present in relevant figure legends (or in the Methods section if additional space is needed).

n/a	Confirmed	
☐	☒	The exact sample size (*n*) for each experimental group/condition, given as a discrete number and unit of measurement (animals, litters, cultures, etc.)
☐	☒	A description of how samples were collected, noting whether measurements were taken from distinct samples or whether the same sample was measured repeatedly
☐	☒	A statement indicating how many times each experiment was replicated
☐	☒	The statistical test(s) used and whether they are one- or two-sided (note: only common tests should be described solely by name; more complex techniques should be described in the Methods section)
☐	☒	A description of any assumptions or corrections, such as an adjustment for multiple comparisons
☐	☒	The test results (e.g. *P* values) given as exact values whenever possible and with confidence intervals noted
☐	☒	A clear description of statistics including central tendency (e.g. median, mean) and variation (e.g. standard deviation, interquartile range)
☐	☒	Clearly defined error bars

See the web collection on statistics for biologists for further resources and guidance.

Software

Policy information about availability of computer code

7. Software

Describe the software used to analyze the data in this study.	Statistical analysis was performed with GraphPad Prism 5.0. FACS were analyzed with CytExpert 1.0 (BECKMAN). VSV-GFP were quantified with Image J 1.51k.

For manuscripts utilizing custom algorithms or software that are central to the paper but not yet described in the published literature, software must be made available to editors and reviewers upon request. We strongly encourage code deposition in a community repository (e.g. GitHub). *Nature Methods* guidance for providing algorithms and software for publication provides further information on this topic.

Materials and reagents

Policy information about availability of materials

8. Materials availability

Indicate whether there are restrictions on availability of unique materials or if these materials are only available for distribution by a for-profit company.	No restrictions on availability of any materials.

9. Antibodies

Describe the antibodies used and how they were validated for use in the system under study (i.e. assay and species).	Antibodies used for immunoprecipitation (IP), immunoblotting (IB) and immunofluorescence (IF) were as follows: EGFR antibody (#4267S, Cell Signaling, 1:1,000 for IB), EGFR antibody (ab231, Abcam, 1:1,000 for IB), Phospho-EGF Receptor (Tyr1068) Antibody (#3777S, Cell Signaling, 1:1,000 for IB), MEKK2 antibody (ab33918, Abcam, 1:1,000 for IB), Flag-tag antibody (M2, Sigma, 1:5,000 for IB), HA-tag antibody (Y-11, sc-805, Santa Cruz Biotechnology, 1:1,000 for IB and 1:200 for IF), Myc-tag antibody (a-14, sc-789, Santa Cruz Biotechnology, 1:1,000 for IB), IRF3 rabbit mAb (#11904, Cell Signaling, 1:1,000 for IB and 1:200 for IF), phospho-IRF3 (Ser396) rabbit mAb (#4947, Cell Signaling, 1:1,000 for IB), TBK1 rabbit mAb (#3504, Cell Signaling, 1:1,000 for IB), phospho-TBK1 (S172) rabbit mAb (#5483, Cell Signaling, 1:1,000 for IB), Importin α5 (18137-1-AP, Proteintech, 1:1,000 for IB), Importin β1 (#51186, Cell Signaling, 1:1,000 for IB), VSV-G (ABGENT, AP1016a, 1:1,000 for IB). Secondary anti-mouse or anti-rabbit antibodies conjugated to HRP (Amersham Biosciences, 1:10,000 for IB), Secondary AlexaFluor488-labeled anti-rabbit antibody (Molecular Probes R37116, 1:300 for IF) or AlexaFluor593-labeled anti-mouse antibody (Molecular Probes R3712, 1:300 for IF). The polyclonal antibody against phospho-Serine 173 of IRF3 was generated by GL Biochem (Shanghai) Ltd. by immunizing rabbits with Cys-PQPLRp(S)PSLDNPT peptide. All antibodies have been described as required in Methods and validated by Western blotting.

10. Eukaryotic cell lines

a. State the source of each eukaryotic cell line used.	All cell lines were originally obtained from ATCC.
b. Describe the method of cell line authentication used.	None of the cell lines have been authenticated.
c. Report whether the cell lines were tested for mycoplasma contamination.	"All cell lines tested negative for mycoplasma contamination" has been declared in Methods.
d. If any of the cell lines used are listed in the database of commonly misidentified cell lines maintained by ICLAC, provide a scientific rationale for their use.	No commonly misidentified cell lines were used.

Animals and human research participants

Policy information about studies involving animals; when reporting animal research, follow the ARRIVE guidelines

11. Description of research animals

Provide details on animals and/or animal-derived materials used in the study.	For in vivo viral infection studies, 8-week-old control and mutant mice were intraperitoneal injected with VSV (5 × 108 pfu/mouse) or intranasal administrated with HSV-1 (2 × 107 pfu/mouse).Details of animals and animal-derived materials were described in Methods.

Policy information about studies involving human research participants

12. Description of human research participants

Describe the covariate-relevant population characteristics of the human research participants.	9 lung cancer patients (40-59 years age, mean=53 years) and 13 non-cancer patients (40-62 years age, mean=55 years) had confirmed influenza infection at Chonqing Medical University were selected. Details of human research participants were described in Methods.

nature research

Corresponding author(s): Fangfang Zhou, Long Zhang

☐ Initial submission ☐ Revised version ☒ Final submission

Flow Cytometry Reporting Summary

Form fields will expand as needed. Please do not leave fields blank.

Data presentation

For all flow cytometry data, confirm that:

☒ 1. The axis labels state the marker and fluorochrome used (e.g. CD4-FITC).

☒ 2. The axis scales are clearly visible. Include numbers along axes only for bottom left plot of group (a 'group' is an analysis of identical markers).

☒ 3. All plots are contour plots with outliers or pseudocolor plots.

☒ 4. A numerical value for number of cells or percentage (with statistics) is provided.

Methodological details

5. Describe the sample preparation.	20 µg exosomes were mixed with 5 µl 4-um aldehyde/sulphate latex beads (Invitrogen, lot:1743119) in 500 µl 1XPBS for 30 min at room temperature with continuous rotation. Exosomes-bound beads were incubated with 1 µg PE IgG Control (#555743, BD) or 1µg PE anti-EGFR antibody (#555997, BD) for 30min. For cells flow cytometry, THP1 or A549 were incubated with 1 µg PE IgG Control or 1 µg PE anti-EGFR antibody for 30 min in DMEM.
6. Identify the instrument used for data collection.	Beckman CytoFlex
7. Describe the software used to collect and analyze the flow cytometry data.	CytExpert Software
8. Describe the abundance of the relevant cell populations within post-sort fractions.	PE postive populations indicates that cells or exosomes contains EGF receptor.
9. Describe the gating strategy used.	Boundaries are defined between PE postive exosomes population ("positive") and PE negative exosomes population ("negative").

Tick this box to confirm that a figure exemplifying the gating strategy is provided in the Supplementary Information. ☒